Fall 1-31-1975

Design of a YIG-tuned oscillator

Tien Liang Jin
New Jersey Institute of Technology

Copyright Warning & Restrictions

The copyright law of the United States (Title 17, United States Code) governs the making of photocopies or other reproductions of copyrighted material.

Under certain conditions specified in the law, libraries and archives are authorized to furnish a photocopy or other reproduction. One of these specified conditions is that the photocopy or reproduction is not to be "used for any purpose other than private study, scholarship, or research." If a, user makes a request for, or later uses, a photocopy or reproduction for purposes in excess of "fair use" that user may be liable for copyright infringement,

This institution reserves the right to refuse to accept a copying order if, in its judgment, fulfillment of the order would involve violation of copyright law.

Please Note: The author retains the copyright while the New Jersey Institute of Technology reserves the right to distribute this thesis or dissertation

Printing note: If you do not wish to print this page, then select "Pages from: first page # to: last page #" on the print dialog screen

DESIGN OF A YIG-TUNED OSCILLATOR

BY

TIEN LIANG JIN

A THESIS

PRESENTED IN PARTIAL FULFILLMENT OF

THE REQUIREMENTS FOR THE DEGREE

OF

MASTER OF SCIENCE IN ELECTRICAL ENGINEERING

AT

NEW JERSEY INSTITUTE OF TECHNOLOGY

Newark, New Jersey
1975

ABSTRACT

A technique for designing YIG (yttrium-iron garnet)-tuned transistor oscillators, tunable over the range of frequencies from 500 to 950 MHZ, is presented. The approach taken differs appreciably from that used in the design of conventional LC-tuned oscillators. One major difference is that the YIG tuning mechanism is electrically controlled. The YIG tuning element is treated as a single unit and is not resolved into an equivalent LC circuit. Instead, a direct method using reflection coefficients measured at network terminals to characterize various design stages is applied. The transistor is also characterized by reflection and transmission coefficients, i.e., S-parameters. Thus the Smith Chart becomes a useful tool and network calculations are greatly simplified by means of signal flow analysis with application of Mason's rule. Because S-parameters are measured when the device is terminated in the characteristic impedance of the measuring system, they are more accurately determined at high frequencies than other parameters requiring open and short circuit terminations for their measurement. Furthermore, the availability of network analyzers, such as the Hewlett-Packard S-Parameter Test Set, simplifies such measurements. As a result, a concise method using S-parameters is most applicable for the design of transistor YIG-tuned oscillators.

APPROVAL OF THESIS

DESIGN OF A YIG-TUNED OSCILLATOR

BY

TIEN LIANG JIN

FOR

DEPARTMENT OF ELECTRICAL ENGINEERING

NEW JERSEY INSTITUTE OF TECHNOLOGY

BY

FACULTY COMMITTEE

APPROVED: _____

_____

_____

NEWARK, NEW JERSEY

JANUARY, 1975

PREFACE

The purpose of this thesis is to develop a concise method for the design of YIG-tuned oscillators. The first chapter is an introduction to the structure and resonance phenomenon of YIG. A description of the properties and characteristics of YIG resonators is presented in Chapter 2. Design considerations in using YIG as part of a tuning element are also included.

Chapter 3 describes the structure of the electromagnet used to provide the biasing dc magnetic field for the YIG resonator. The design of a YIG-tuned transistor oscillator is analysed in Chapter 4. Smith Charts are used to clarify explanations.

The final chapter summarizes conclusions based on experiments performed and discusses recommendations for future work related to this subject.

It is a great pleasure to thank Dr. Gerald Whitman and Dr. Joseph Frank, project directors, of New Jersey Institute of Technology, for their continued interest, encouragement and helpful suggestions; the staff of Airtron Division of Litton Industries, for their fine cooperation and construction of the YIG mount and electromagnet. Thanks are also due Mr. Frank Peragine, of Bell Laboratories, for providing measured S-parameter

data for type 2N2857 transistors; Mrs. Marguerite Gribbon, of the Foundation at New Jersey Institute of Technology, for typing the original manuscript. Finally, thanks are due Airtron Division of Litton Industries for providing YIG spheres, test equipment, and funding for the project.

The author will very much appreciate having any oversights or errors brought to his attention.

January, 1975 T. L. Jin

TABLE OF CONTENTS

LIST OF FIGURES

LIST OF TABLES

INTRODUCTION

Since its discovery, yttrium-iron garnet (YIG) has been widely used in microwave applications. Some of the major applications for YIG tuned devices include microwave frequency generators, fast scanning preselectors for commercial and military equipment, local oscillators in microwave surveillance receivers, sweep signal sources, frequency synthesizers, and filter resonators. One great advantage of such devices is the linear tuneability due to the resonance property of the YIG material in a dc magnetic field. However, most of these applications involve devices operating in the gigahertzs frequency band.

It is therefore the primary objective of this paper to introduce the fundamental concepts of the structure and behavior of YIG resonators as tuning elements, and to develop a concise method for the design of YIG tuned oscillators operating in the lower microwave or ultra-high frequency band, which coincides with the UHF TV broadcasting band.

CHAPTER 1

YTTRIUM-IRON GARNET (YIG)

1.1. Structure of YIG

Yttrium-iron garnet (YIG), represented by the unit formula $Y_3Fe_2(FeO_4)_3$ or $3Y_2O_3 \cdot 5Fe_2O_3$, is a polycrystalline garnet prepared by two methods: by ball milling the constituent oxides and by coprecipitation as hydroxides followed by a sintering process. In the former method, the reacted powders obtained by presintering in an oxygen atmosphere are ball milled, pressed into shape and then sintered in an oxygen atmosphere. This method produces specimens with higher densities. Toroidal specimens prepared from oxides presintered at 950 °C attained densities as high as 99% of the theoretical density {1}.

The crystal structure of the garnets consists of cubic unit cells each made up of eight of the formula units $Y_3Fe_2(FeO_4)_3$. Sixteen Fe^{3+} ions occupy octahedral sites, called a-sites, each at the center of an octahedron. These sites represent magnetic A sublattices. Twenty-four Fe^{3+} ions occupy d-sites each at the center of a tetrahedron, forming the magnetic D sublattice. The Y^{3+} ions occupy twenty-four c-sites, each at the center of an 8-cornered 12-sided polyhedron, as shown in Fig. 1.1.1.

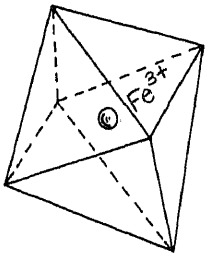

(a) Fe^{3+} ion surrounded by six oxygen ions in octahedral symmetry.

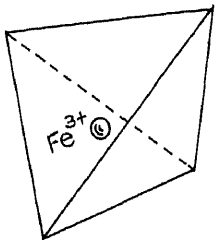

(b) Fe^{3+} ion surrounded by four oxygen ions in tetrahedral symmetry.

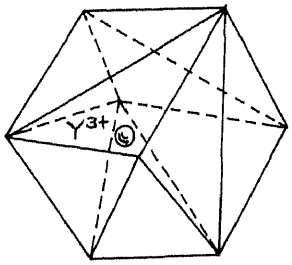

(c) Y^{3+} ion surrounded by eight oxygen ions in the 8-corners of a 12-sided polyhedron.

Fig. 1.1.1. (a) a-site, (b) d-site, (c) c-site of YIG crystal {16}.

The 96 oxygen ions in the unit cell occupy the h-sites which correspond to a point where a corner of a tetrahedron, octahedron, and two large polyhedra meet, as shown in Fig. 1.1.2.

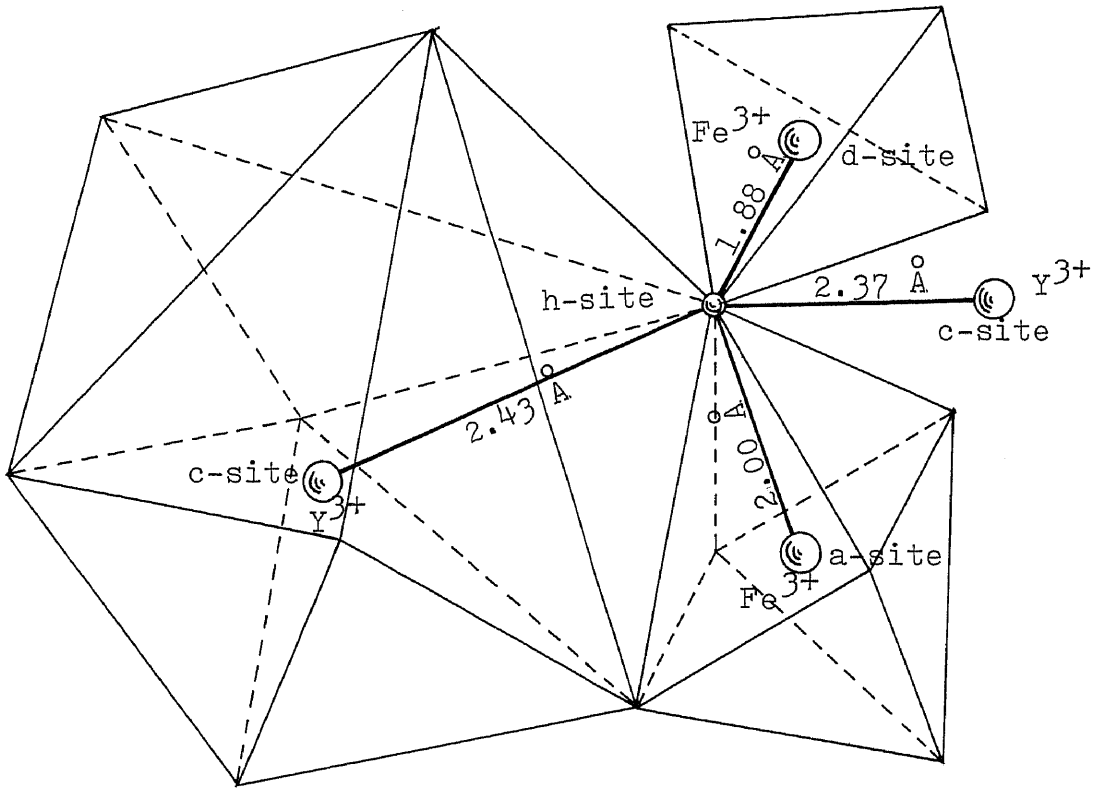

Fig. 1.1.2. Distances (in Angstrom units) of each metal ion from common oxygen neighbor (h-site) for YIG {16}. (second large polyhedron not shown)

Thus, each oxygen ion is surrounded by an Fe^{3+} (a-site) ion, an Fe^{3+} (d-site) ion, and two Y^{3+} (c-site) ions. However, these are not regular polyhedra because the corresponding sides of each geometrical figure are not always equal {16}.

Polycrystalline garnets may also be fabricated by partial substitution for yttrium or iron in YIG. These garnets can be represented by two generalized chemical formulas. The formula $3Y_2O_3(5-x)Fe_2O_3 \cdot xGa_2O_3$, where x varies from 0 to 1, represents the series of garnets in which varying amounts of gallium substitute for iron in the tetrahedral sites; the formula $(3-x)Y_2O_3 \cdot xR_2O_3 \cdot 5Fe_2O_3$, where R is a rare earth and x varies from 0 to 3, represents the series in which rare earth ions substitute for yttrium. The lattice constant of polycrystalline YIG was determined to be 12.374 ± 0.005 Å. Some slight variations in the lattice constant were found in samples in which rare earth ions replace the yttrium ions {1}.

The magnetic properties of the garnet result from the superexchange interactions between pairs of sub-lattices. The strongest interactions occur when the angle between the magnetic ions approaches 180 degrees, and the weakest for angles near 90 degrees. Thus, a stronger A-D sublattices interaction is expected because the angle $Fe^{3+}(a)\text{-}O^{2-}\text{-}Fe^{3+}(d)$ formed by the Fe^{3+} ions in

the two sublattices is 126.6°. Such interaction is strong enough to permit considerable overlap of the wave functions of oxygen and iron. A weaker coupling between Y^{3+} and $Fe^{3+}(a)$ can be explained by the smaller Y^{3+}-O^{2-}-$Fe^{3+}(a)$ angle of 100° {16}.

Since the trivalent yttrium, Y^{3+}, consisting of the inert Krypton core, has its 4p layer completely filled with electrons, there are no unpaired spins. Thus Y^{3+} has no permanent spin magnetic moment. Therefore, the net magnetization of YIG is contributed by the difference between the magnetic moments of $3Fe^{3+}(d)$ ions and the $2Fe^{3+}(a)$ ions, each having a magnetic moment of 5 Bohr magnetons ($5\mu_B$). Because of the dominant D sublattice, there is a net magnetization of 5 Bohr magnetons per formula unit of YIG {16}.

1.2. Motion of the Magnetization Vector

Consider a single-crystal YIG sphere in a dc magnetic field. If the dc field of strength H_o is applied to the sphere in a vertical z-direction, the magnetic moment $\bar{\mu}$ due to the spinning of the unpaired electrons in the YIG material will precess about $\bar{H}_o$. The precessional frequency ω_o will depend upon the associated angular momentum $\bar{J}$. This angular momentum and the magnetic moment $\bar{\mu}$ are parallel vectors. For the electron, they are

oppositely directed and the gyromagnetic ratio is thus defined by

$$\gamma_o = -\mu/J , \qquad (1.2.1)$$

where $\gamma_o = 2.21 \times 10^5$ (rad/sec)/(A-t/m), and $\mu = -eh/2m$, with e the absolute value of the electronic charge, m its mass and h, Planck's constant.

Under equilibrium conditions, the dipole moment vector $\bar{\mu}$ lies in the direction opposite to that of $\bar{H}_o$. Now suppose that the magnetic dipole moment is tilted by a small external force so that it makes an angle θ with $\bar{H}_o$. A torque $\bar{T}$ is then exerted on the spinning electron and its angular momentum vector $\bar{J}$ precesses about a cone with angular velocity $\omega_o = d\phi/dt$, as shown in Fig. 1.2.1.

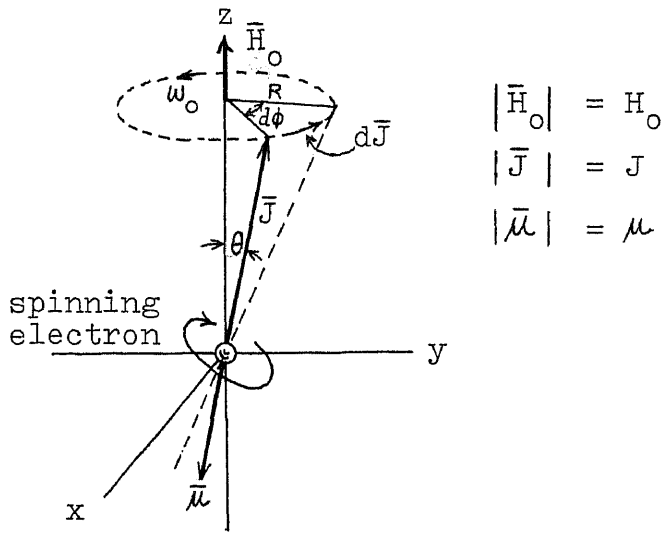

Fig. 1.2.1. Precession of magnetic moment about the dc magnetic field [14].

The time rate of change of the angular momentum vector is equal to the torque, i.e.,

$$\bar{T} = \frac{d\bar{J}}{dt} \ . \qquad (1.2.2)$$

In the time interval dt, the change in angular momentum is $\bar{T}$ dt and the change in ϕ is $d\phi$. The angle $d\phi$ is equal to the arc dJ divided by the radius of the precession circle J sin θ; thus,

$$d\phi = \frac{dJ}{J \sin \theta} = \frac{T \ dt}{J \sin \theta} \ ,$$

i.e.,

$$\frac{d\phi}{dt} = \omega_o = \frac{T}{J \sin \theta} \ . \qquad (1.2.3)$$

Since T = dJ/dt,

$$\frac{dJ}{dt} = \omega_o J \sin \theta \ , \qquad (1.2.4.a)$$

or in vector notation as

$$\frac{d\bar{J}}{dt} = \bar{\omega}_o \times \bar{J} \ , \qquad (1.2.4.b)$$

where $\bar{\omega}_o = \hat{z}\omega_o$ with $\hat{z}$ a unit vector in the z-direction.

Since the only field acting on $\bar{\mu}$ is $\bar{H}_o$, the torque exerted on $\bar{\mu}$ is

$$\bar{T} = \bar{\mu} \times \bar{H}_o \ . \qquad (1.2.5)$$

From equations (1.2.2) and (1.2.1), the torque can also

be written as

$$\bar{T} = \frac{d\bar{J}}{dt} = -\frac{1}{\gamma_o}\frac{d\bar{\mu}}{dt} \quad . \qquad (1.2.6)$$

Combining equations (1.2.5) and (1.2.6) gives the equation of motion of a single dipole:

$$\frac{d\bar{J}}{dt} = -\gamma_o \bar{J} \times \bar{H}_o = \gamma_o \bar{H}_o \times \bar{J} \qquad (1.2.7.a)$$

and

$$\frac{d\bar{\mu}}{dt} = -\gamma_o \bar{\mu}_o \times \bar{H}_o = \gamma_o \bar{H}_o \times \bar{\mu} \; . \qquad (1.2.7.b)$$

Equations (1.2.4.b) and (1.2.7.a) establish the relation

$$\bar{\omega}_o = \gamma_o \bar{H}_o \qquad (1.2.8)$$

as the natural precession frequency of a magnetic dipole in a constant magnetic field.

The total magnetization of a system of magnetically aligned spins is given by

$$\bar{M} = N\bar{\mu} \; ,$$

where N is the number of unbalanced spins per unit volume {14}. Equation (1.2.7.b) now becomes

$$\frac{d\bar{M}}{dt} = -\gamma_o (\bar{M} \times \bar{H}_o) \; . \qquad (1.2.9.a)$$

Usually only the absolute value of the electronic charge is used in defining μ. As a consequence, $\bar{M}$ in equation (1.2.9.a) becomes negative and can be written as

$$\frac{d\bar{M}}{dt} = \gamma_o(\bar{M} \times \bar{H}_o) \qquad (1.2.9.b)$$

where

γ = ge/2mc

g = Landé g factor ≈ 2

m = mass of the electron

e = absolute value of the electronic charge

c = velocity of light

$\gamma_o = \mu_o \gamma$

μ_o = intrinsic permeability of free space

$\bar{M}$ = magnetization vector

$\bar{H}_o$ = applied magnetic field vector

1.3. Damping and Resonance Phenomenon

The precession frequency of the magnetization vector about the constant magnetic field is determined by the field strength. Because of damping, the electron-spin magnetic moments will spiral in until the magnetization aligns itself with the H_o field. By sampling the fields around the sphere during this process, a circularly polarized rf field would be observed about the sphere. This field would die out exponentially with time in the same way that transient voltages and currents die out in a resonant circuit having dissipation loss [18].

Magnetic loss or damping takes two basic forms:

the Bloch-Bloembergen (B-B) form and the Landau-Lifshitz (L-L) form. The B-B form of the equation of motion is given by

$$\left(\frac{d\bar{M}}{dt}\right)_{x,y} = \gamma_o (\bar{M} \times \bar{H})_{x,y} - \frac{M_{x,y}}{T_2} \qquad (1.3.1.a)$$

$$\left(\frac{d\bar{M}}{dt}\right)_{z} = \gamma_o (\bar{M} \times \bar{H})_{z} - \frac{M_z - M_o}{T_1} , \qquad (1.3.1.b)$$

where

$\bar{H}$ = magnetic field vector

T_1 = spin-lattice relaxation time

T_2 = loss associated with any process that disturbs or opposes the precessional motion

$\bar{M}$ = magnetization vector

M_o = dc magnetization

x,y,z = subscripts indicating the x,y, and z components of the vector.

The L-L form is given by

$$\frac{d\bar{M}}{dt} = \gamma_o (\bar{M} \times \bar{H}) - \lambda \frac{(\bar{H}\cdot\bar{M})\bar{M}}{M^2} - \bar{H} , \qquad (1.3.2)$$

where λ is a damping factor with dimensions of frequency called the relaxation frequency, and is the inverse of a relaxation time. Since $\bar{M}\cdot\bar{M} = M^2$, equation (1.3.2) can be rearranged as

$$\frac{d\bar{M}}{dt} = \gamma_o(\bar{M} \times \bar{H}) - \frac{\lambda}{M^2}\left[(\bar{H}\cdot\bar{M})\bar{M} - (\bar{M}\cdot\bar{M})\bar{H}\right]. \quad (1.3.2.a)$$

After applying the vector identity

$$\bar{A} \times (\bar{B} \times \bar{C}) = \bar{B}(\bar{A}\cdot\bar{C}) - \bar{C}(\bar{A}\cdot\bar{B}) \quad (1.3.3)$$

to the equation, it becomes

$$\frac{d\bar{M}}{dt} = \gamma_o(\bar{M} \times \bar{H}) - \frac{\lambda}{M^2}\left[\bar{M} \times (\bar{M} \times \bar{H})\right]. \quad (1.3.2.b)$$

Equation (1.3.2.b) shows that the damping term is a vector perpendicular to $\bar{M}$. Therefore, the damping term affects only the precession angle. The magnitude of the magnetization vector remains unaffected {16}.

However, the precession can be sustained by superimposing a small rf magnetic field in the plane perpendicular to the dc magnetic field as shown in Fig. 1.3.1. When the frequency of the rf magnetic field, h_{rf}, coincides with the natural precession frequency of the magnetization, the precession angle will grow in size. The energy absorbed from the rf magnetic field by the spins will go through a maximum until further growth in angle is limited by damping. Thus, to observe the resonance condition, the operating frequency or the applied dc magnetic field can be varied until the driving frequency equals the natural precession frequency {16}.

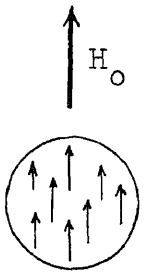

(a) Magnetic dipoles aligned in direction of applied dc field.

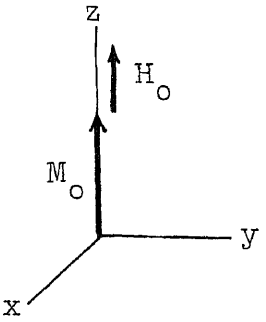

(b) Net magnetization produced by combined effects of aligned dipoles.

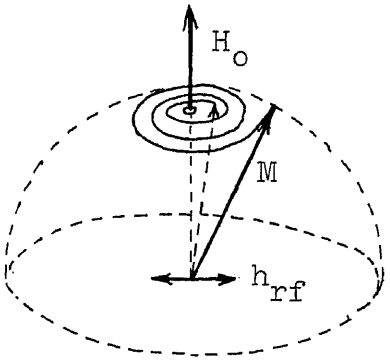

(c) Precession of magnetization vector under influence of applied rf field with $\omega = \omega_o$.

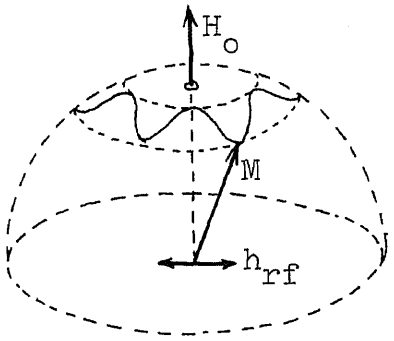

(d) Oscillations of magnetization vector under influence of applied rf field with $\omega \neq \omega_o$.

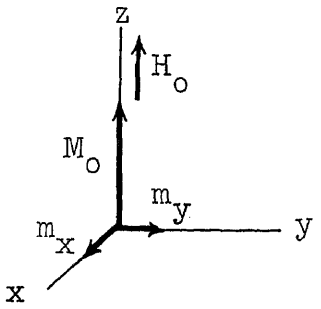

(e) Components of the precessing magnetization vector.

Fig. 1.3.1. Effects of rf magnetic field applied in the plane perpendicular to the dc magnetic field {16}.

When the frequency of the rf magnetic field is not equal to the natural precession frequency, oscillations of the magnetization vector {16}, as shown in Fig. 1.3.1 (d), result.

CHAPTER 2

FERRIMAGNETIC RESONATORS

2.1. Characteristics of Ferrimagnetic Resonators

The physical parameters that affect the design of ferrimagnetic resonators are the Curie temperature T_c, the saturation magnetization M_s, the anisotropy field constant K_1/M_s, and the resonance line width ΔH [18].

2.1.1. Curie Temperature T_c

The Curie temperature is the temperature at which the saturation magnetization M_s drops to zero. Therefore, resonance operation near or above this temperature is impossible.

2.1.2. Saturation Magnetization M_s

The saturation magnetization M_s is determined by the number of electron spins per unit volume of the material. It is a measure of the ease with which the fields associated with external circuitry can couple to the resonator; the larger the M_s, the easier the coupling. Furthermore, the saturation magnetization and the shape of the resonator determine the minimum resonant frequency, f_o^{min}, which saturates the material. If a resonator is tuned to a frequency lower than f_o^{min}, the

applied field would be approximately equal to or less than the demagnetizing field. In such a case the resonator would cease to function. The relationship between the approximate minimum resonant frequency f_o^{min} and the saturation magnetization M_s is shown in Fig. 2.1.2.1 {18}.

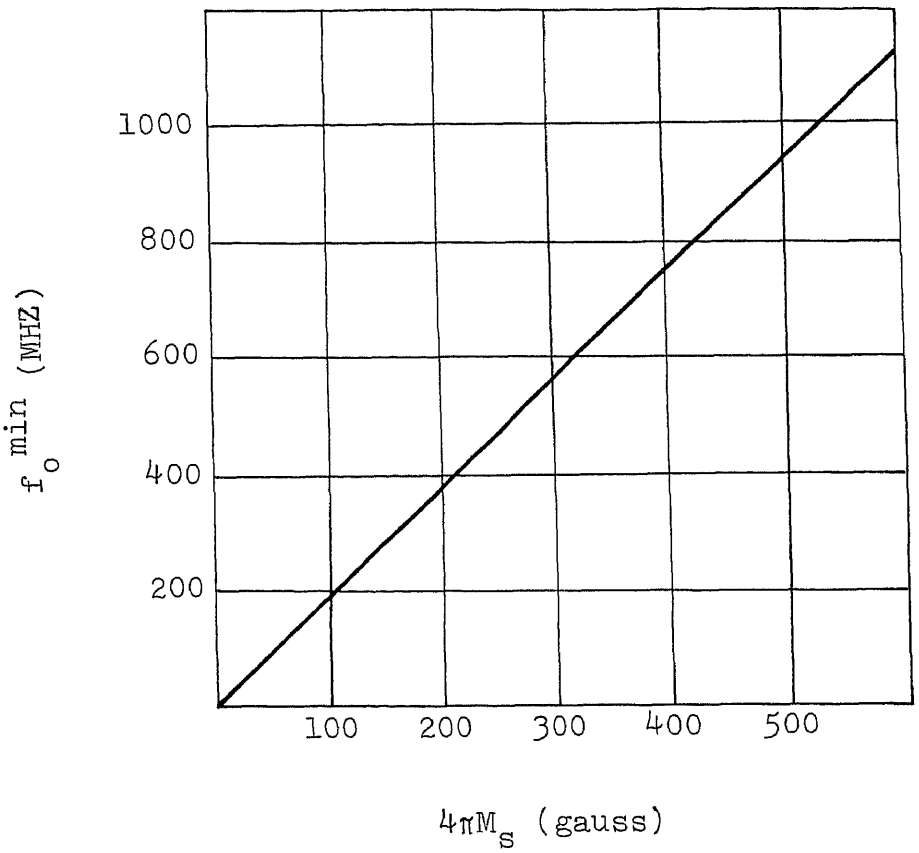

Fig. 2.1.2.1. Approximate minimum resonant frequency of ferrimagnetic sphere.

2.1.3. Anisotropy Field Constant K_1/M_s

Since YIG and GaYIG have cubic crystal structure, they have three types of principal axes: three [100], six [110] and four [111] axes in each single crystal. The lattice structure of the single-crystal material gives rise to the effects of magneto-crystalline anisotropy, which is represented by the first-order anisotropy field constant K_1/M_s. This is a measure of the ease with which the crystal magnetizes along certain crystal axes rather than along others. Therefore, the biasing magnetic field required to produce resonance depends upon the orientation of the crystal axis with respect to the applied magnetic field. For YIG or GaYIG, the lowest field strength that gives resonance occurs when a [111] axis is parallel to the applied field. The opposite effect occurs when a [100] axis is parallel to the applied field. Therefore, the [111] axes are known as "easy" axes while the [100] axes are known as "hard" axes. Second-order anisotropy field constant also exists; however, its effect on resonance is negligible {18}.

The variations of biasing magnetic field, for a single-crystal YIG or GaYIG having cubic symmetry, as a function of crystal axes orientation, are shown in Fig. 2.1.3.1 and given by the equation,

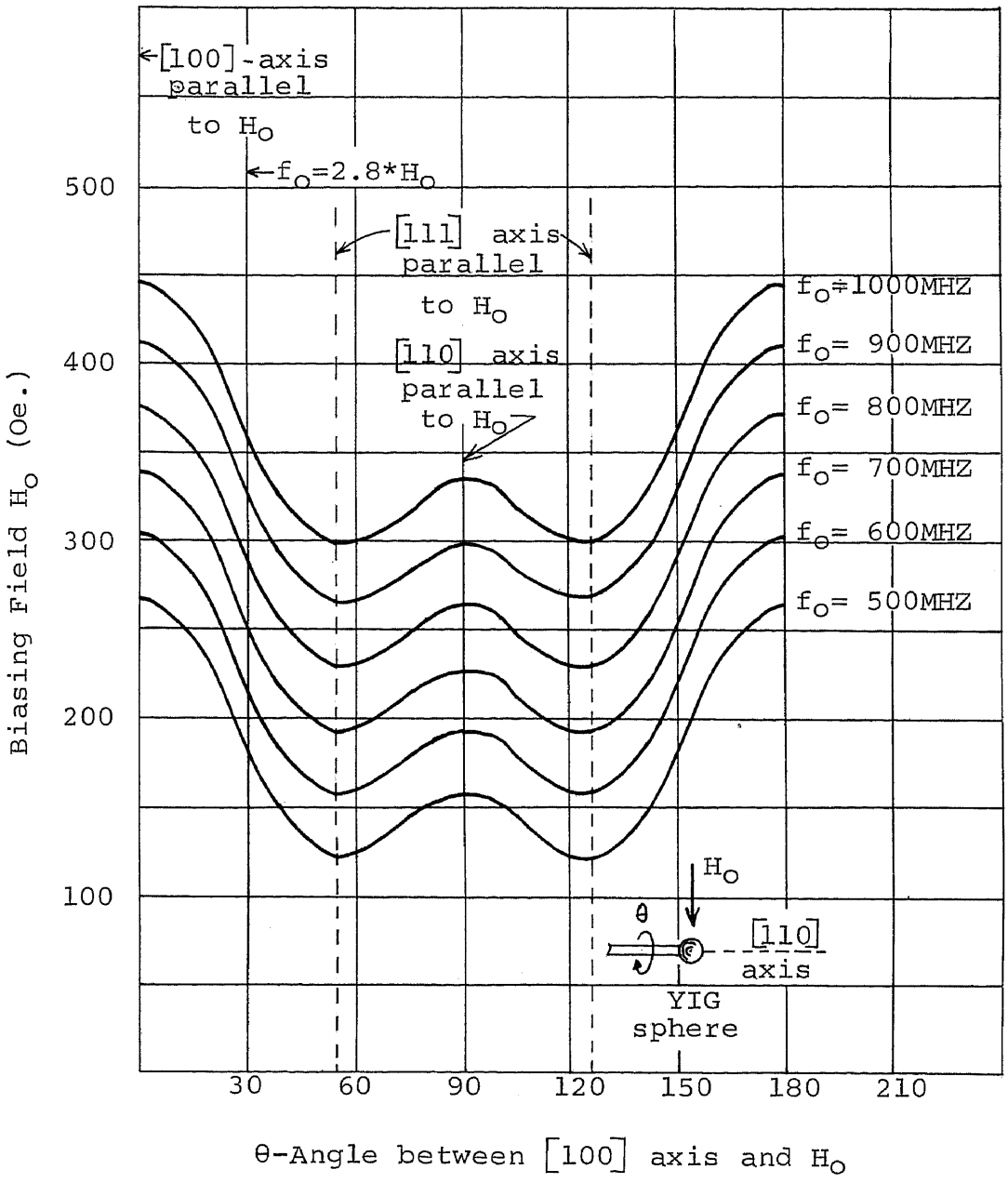

Fig. 2.1.3.1 Field strength required to give resonance as a YIG sphere is rotated about a [110] axis which is perpendicular to H_o.

$$H_o = H_{eff} - \left(2 - \frac{5}{2} \sin^2\theta - \frac{15}{8} \sin^2 2\theta \right) \frac{K_1}{M_s}, \text{oersteds,} \qquad (2.1.3.1)$$

where

$$H_{eff} = \frac{f_o}{2.8}, \text{ oersteds,} \qquad (2.1.3.1.a)$$

and

f_o = resonant frequency in MHZ

K_1/M_s = first-order anisotropy field constant.

θ is the angle between the applied magnetic field H_o and the [100] axis which becomes parallel to H_o as the sphere is rotated about the given [110] axis. Orientation of a particular axis with respect to the biasing magnetic field can be achieved by rotating the sphere around a [110] axis which is perpendicular to the applied field {6}.

The [110] axis can be determined by X-ray techniques or by using the device developed by Y. Sato and P.S. Carter {21}. The operating principle of this device is based on the method proposed by M. Auer {4}. The device consists of an electromagnet placed on a rotating mount. Thus the field can be oriented in any desired direction with respect to the crystal sphere. The sphere is placed on a dimpled rod in such a way

that it is free to rotate. When the sphere is subjected to a strong magnetic field, it will rotate until one of its easy [111] axis aligns itself in the direction of the applied field. A wire is temporarily attached to the sphere along the direction of this axis. Next, the wire is placed in a radial hole, where it is free to rotate, at the side of the aligning jig. The magnet is then rotated 70.5 degrees from its original position. This angle can accurately be measured by means of the milling head protractor of the device. Now the sphere rotates around the wire until the second easy axis aligns itself with the field.

Finally, an insulating rod is attached with a drop of cement to the sphere along the [110] axis. This is done by means of the radial hole drilled at the side of the alignment jig along the bisector of the angle between the two easy axes. Fig. 2.1.3.2 shows the geometry of a cubic crystal structure.

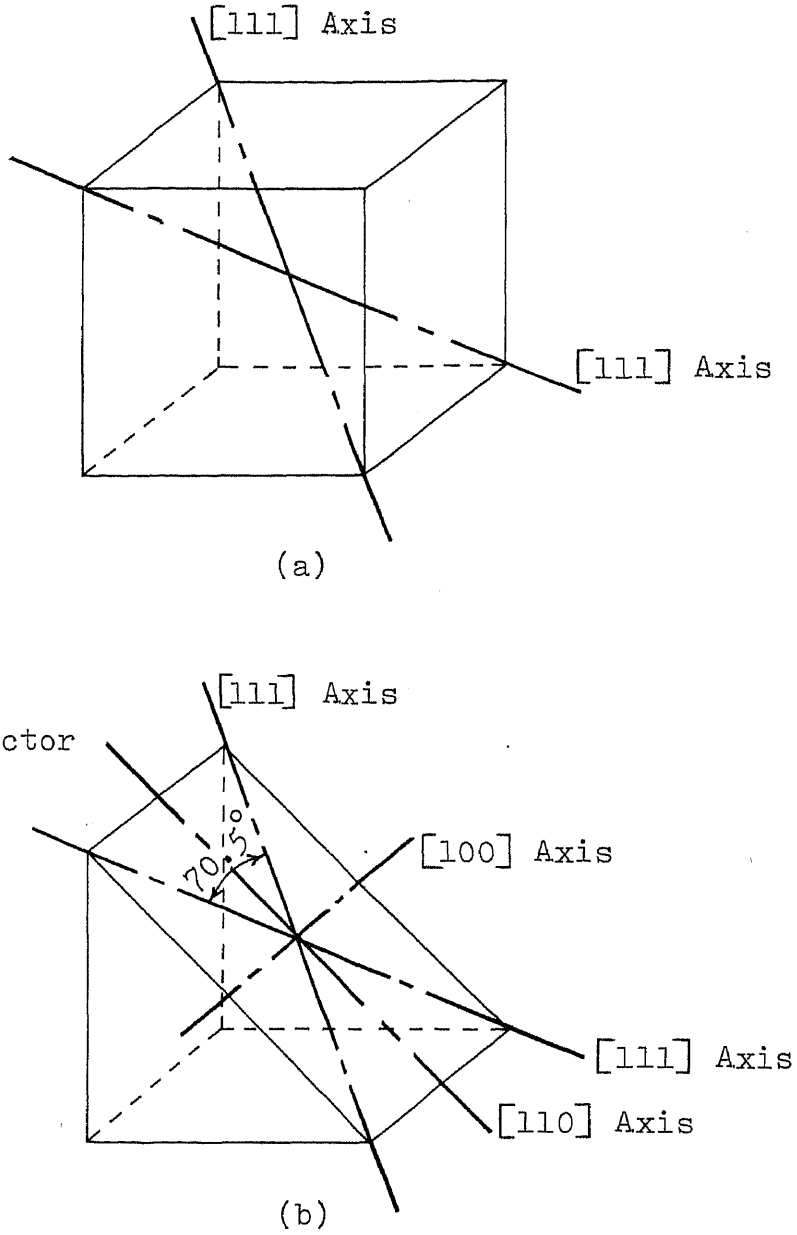

Fig. 2.1.3.2. Geometry of a cubic crystal. (a) cubic crystal whose body diagonals are easy axes, (b) cutoff section of cubic crystal showing relative locations of crystal axes.

2.1.4. Line Width ΔH

Another property of the ferrimagnetic material is the resonance line width ΔH, which depends upon the shape and surface polish of the material. To achieve the narrowest possible line width, the internal field of the material must be uniform and the surface of the resonator must be very highly polished. However, the line width, though independent of the external circuits, may be degraded if located near metallic walls [18].

The theoretical unloaded Q, Q_u, is a function of the line width and is defined by [6]

$$Q_u = \frac{f_o}{2.8\,\Delta H} \quad , \qquad (2.1.4.1)$$

where

f_o = resonant frequency in MHZ

ΔH = line width in oersteds.

However, when a homogeneous specimen is placed in a uniform magnetic field, it becomes polarized. The polarization induces magnetic dipoles at the surface and creates a component of the magnetic field opposing the applied field. This induced field is given by

$$H_d = N_z M_o \, , \qquad (2.1.4.2)$$

where

H_d = induced field

N_z = demagnetizing factor in the direction of the applied field

M_o = d.c. magnetization

The demagnetizing factor N measures the degree of induction and depends upon the shape of the resonator. For spheres, these factors are $N_x = N_y = N_z = 1/3$, where the subscripts x, y, and z denote the direction of the axes of the chosen rectangular coordinate system shown in Fig. 2.1.4.1 {16}.

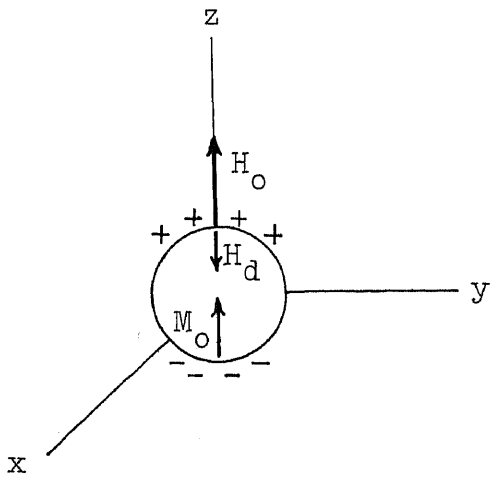

Fig. 2.1.4.1. Polarization of a homogeneous specimen in a uniform magnetic field.

Taking the effects of the demagnetizing field into account, the unloaded Q is given by equation (2.1.4.2) {7}.

$$Q_u = \frac{f_o - f_d}{2.8\,\Delta H} \qquad (2.1.4.2.a)$$

$$= \frac{H_o - H_d}{\Delta H} = \frac{H_o - N_z M_o}{\Delta H} \qquad (2.1.4.2.b)$$

$$= \left(\omega_o - N_z \omega_m\right) \frac{\tau}{2} , \qquad (2.1.4.2.c)$$

where ΔH is the line width defined by

$$\Delta H = \frac{2}{\gamma_o \tau} \qquad (2.1.4.3)$$

and

$$\omega_m = \gamma_o M_o . \qquad (2.1.4.4)$$

τ is the Bloch-Bloembergen phenomenological relaxation time and the rest of the symbols are as previously defined.

2.2. Single-loop Coupled Resonator

The coupling of small ferrimagnetic spheres to two orthogonal loops or semi-loops has been analyzed by Comstock {10}. The results are summarized below.

A YIG sphere is placed in the center of two loops. The loop axes are perpendicular to each other and to the direction of the applied dc magnetic field, as shown in

Fig. 2.2.1.

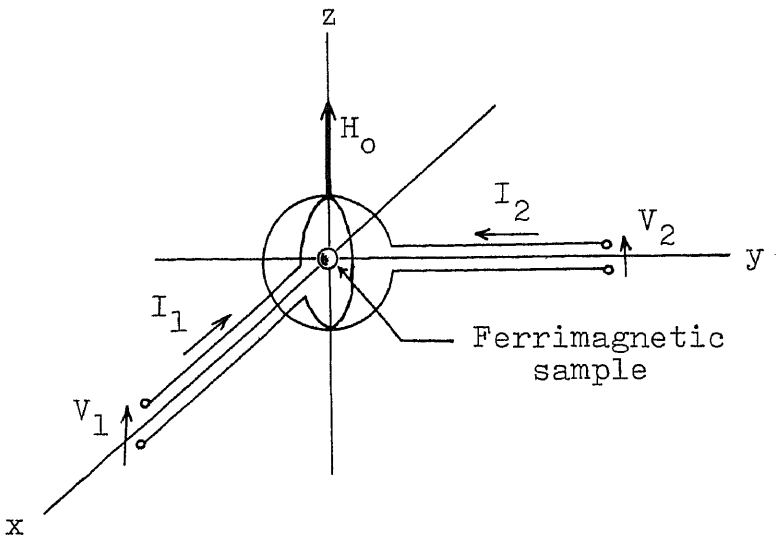

Fig. 2.2.1. Loop coupling by a ferrimagnetic sphere.

With no external field there is little coupling between the input and output terminals since the loops are orthogonal to each other. However when a dc magnetic field is applied, coupling through the magnetized YIG sphere takes place. The amount of coupling depends upon the input rf signal frequency and the dc magnetic field strength. Signals at the gyromagnetic resonance frequency, $f_o = 2.8 \times H_o$, are strongly coupled while at other frequencies the coupling is quite weak.

In the case where loop coupling is used, voltages V_1 and V_2 developed around the loops are shown to be {10}

$$\begin{bmatrix} V_1 \\ V_2 \end{bmatrix}_{loop} = j\omega\mu_o \frac{v_s}{2r_o^2} \begin{bmatrix} X^e_{xx} I_1 + X^e_{xy} I_2 \\ X^e_{yx} I_1 + X^e_{yy} I_2 \end{bmatrix}, \quad (2.2.1)$$

where I_1 and I_2 are the currents flowing in the loops and

ω = radian frequency

μ_o = intrinsic permeability of free space

v_s = volume of sphere

r_o = radius of coupling loop

$X^e_{xx} = X^e_{yy}$ = (x-x), (y-y) component of effective rf tensor susceptibility

$X^e_{xy} = -X^e_{yx}$ = (x-y), (y-x) component of effective rf tensor susceptibility.

The effective or external susceptibility is the ratio of the rf magnetic moment to the applied rf magnetic field (not the rf magnetic field inside the ferrite). For a spherical sample the approximate expressions for the components of the effective rf tensor susceptibility are given by [7]

$$X^e_{xx} = X^e_{yy} = \frac{\omega_o \omega_m}{\omega_o^2 - \omega^2 + \frac{2j\omega}{\tau}\left(1 + \frac{\omega_m/3}{\omega_o - \omega_m/3}\right)} \quad (2.2.2.a)$$

$$X^e_{xy} = -X^e_{yx} = \frac{-j\omega_m\omega}{\omega_o^2 - \omega^2 + \frac{2j\omega}{\tau}\left(1 + \frac{\omega_m/3}{\omega_o - \omega_m/3}\right)} \cdot$$

(2.2.2.b)

The external Q, Q_e, of ferrimagnetic resonators has also been derived. The approximate expression is given by

$$Q_e = \frac{4\, r_o^2\, R_o}{\mu_o v_s \omega_m}\left[1 + \left(\frac{\omega L_\ell}{R_o}\right)^2\right], \qquad (2.2.3)$$

where

r_o = radius of the loop

R_o = terminating resistance connected to the loop

L_ℓ = self-inductance of the loop.

Equation (2.2.3) shows the external Q of the resonator as a function of loop radius.

To derive an expression for single-loop coupling, remove the second loop and let $I_2 = 0$ in equation (2.2.1). V_1 then becomes

$$V_1 = j\omega\mu_o \frac{v_s}{2r_o^2} X^e_{xx} I_1 . \qquad (2.2.4)$$

Dividing by I_1 and substituting the expression for X^e_{xx}

into equation (2.2.4) gives the expression for the impedance at the terminal of a single YIG coupled loop as

$$Z = \frac{V_1}{I_1} = j\omega\mu_o \frac{v_s}{2 r_o^2} \left[\frac{\omega_o \omega_m}{\omega_o^2 - \omega^2 + \frac{2j\omega}{\tau} \left(1 + \frac{\omega_m/3}{\omega_o - \omega_m/3} \right)} \right] \qquad (2.2.5)$$

Figure 2.2.2 shows the results for the evaluation of equation (2.2.5) at various resonant frequencies. It can be seen from the figure that a single YIG coupled loop behaves like a parallel LC resonant circuit.

2.3. Design Considerations

Changes in temperature affect the values of K_1/M_s, M_s, and ΔH; but changes in K_1/M_s have the most adverse effect on the resonant frequency. To minimize the variations in the resonant frequency due to changes in the anisotropy field constant, the resonator sphere must be properly aligned with respect to the applied magnetic field. This orientation of the sphere is determined by the second term of equation (2.1.3.1) which contains the anisotropy field constant K_1/M_s. Notice that if θ

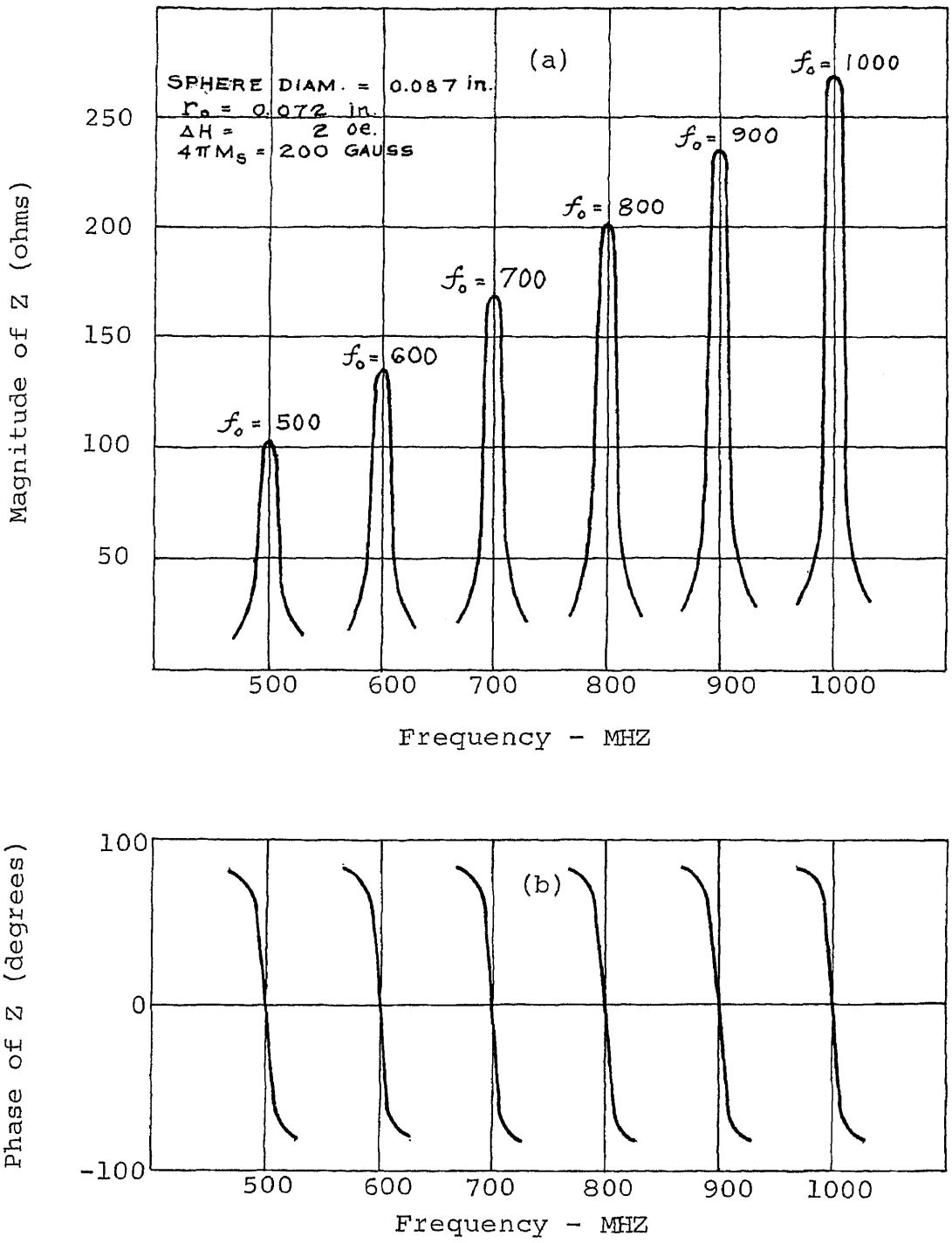

Fig. 2.2.2. Impedance (Z) of single loop coupled to a YIG resonator at various resonant frequencies. (a) magnitude, and (b) phase of Z.

is chosen to be approximately plus or minus 30 degrees, this term becomes very small. Thus the anisotropy effects can be minimized. In this case the resonant frequency is approximately given by $2.8 \times H_o$, where H_o is the applied magnetic field in oersteds. Therefore, frequency variations due to changes in temperature can be minimized {18}.

Higher order magnetostatic modes can be excited when the ferrimagnetic sphere is inhomogeneous or when the applied magnetic field is not uniform. These modes are due to the differences in phases of precession of the magnetic moments in various parts of the sphere sample. They cause spurious resonances which couple to and distort the "main" [110] mode. In order to minimize coupling to the higher order modes, the size of the resonator should be small, so that the field within the sample can be more uniform. Thus the ratio D_m/λ_o, where D_m is the diameter of the resonator sphere and λ_o, the wavelength at the operating frequency, should be as small as possible provided that coupling from external circuits is adequate. Usually, the diameter of the sphere is chosen to be about two orders of magnitude smaller than the rf wavelength {23}.

The size of the coupling-loop is chosen such that the loop-to-sphere ratio is greater than 1.5:1. This

condition minimizes spurious responses. However, the size of the loop must be made as small as possible to minimize the coupling-loop inductance which is necessary to prevent self-resonances {24}.

At the design center frequency of a system tunable over the frequency range from f_1 to f_2, the inductance for the maximun loop size is given by

$$L = \frac{Z_o}{2\pi f_d(\text{GHZ})}, \text{ nH}, \qquad (2.3.1)$$

where

Z_o = impedance terminating the loop (ohms)

f_d = design center frequency (GHZ)

and the design center frequency is defined by

$$f_d = \sqrt{f_1 f_2}\ . \qquad (2.3.2)$$

The condition established by equation (2.3.1) yields minimum coupling variation over the frequency range. Furthermore, it reduces the effects of spurious magneto-static modes by providing the maximum rf loop-to-sphere diameter ratio {23}.

2.4. YIG Tuning Element

The tuning element of the oscillator consists of a single-loop coupled YIG resonator. It is designed to be tunable over the frequency range from 500 to 950 MHZ.

For a YIG sphere to operate in this frequency range, its saturation magnetization, $4\pi M_s$, must not be larger than 265 gausses, as shown in Fig. 2.1.2.1.

Since the YIG sphere has a diameter of 0.087 in., the diameter of the loop is made at least 0.13 in., i.e. (0.087 x 1.5). This condition minimizes in-band spurious responses. However, the maximum loop diameter is limited by the condition set in equation (2.3.1). In this case, the maximum inductance is approximately 12 nH when the terminating impedance is 50 ohms.

The self-inductance of a circular ring of round wire at radio frequencies, for nonmagnetic materials, is given by {15}

$$L = \frac{a}{100}\left[7.353 \log_{10}\left(\frac{16\,a}{d}\right) - 6.386\right] \mu H , \qquad (2.4.1)$$

where

a = mean radius of ring in inches

d = diameter of wire in inches

and

$$a/d > 2.5 \ .$$

Using wire with a diameter of 0.0195 in., the maximum loop diameter obtained from equation (2.4.1) for an inductance of 12 nH is approximately 0.27 in. Therefore, the condition for the choice of the size of the loop is

$$0.13 \text{ in.} < \text{coupling loop diameter} < 0.27 \text{ in.}$$

The YIG tuning element chosen for the oscillator has the following dimensions:

sphere diameter = 0.087 in.
wire diameter = 0.0195 in.
mean diameter of coupling loop = 0.14 in.

The response of the YIG tuning element is measured with an HP 8745A S-Parameter Test Set which forms part of the 8542A Automatic Network Analyzer System. The procedure is outlined below:

(a) apply a fixed current I through the electromagnet (this provides the dc magnetic field).
(b) apply a signal of a certain frequency within a predetermined range about the resonant frequency at the terminals of the loop enclosing the YIG sphere.
(c) measure the reflection coefficient.

(d) change the frequency of the signal and again measure the reflection coefficient. Repeat the process until the entire range of frequencies is covered.

(e) change the current through the electromagnet and determine the next range of frequencies about the new resonant point.

(f) repeat the measurements by following the procedure from step (b) on.

The results obtained from the measurements described above are plotted in Fig. 2.4.1.

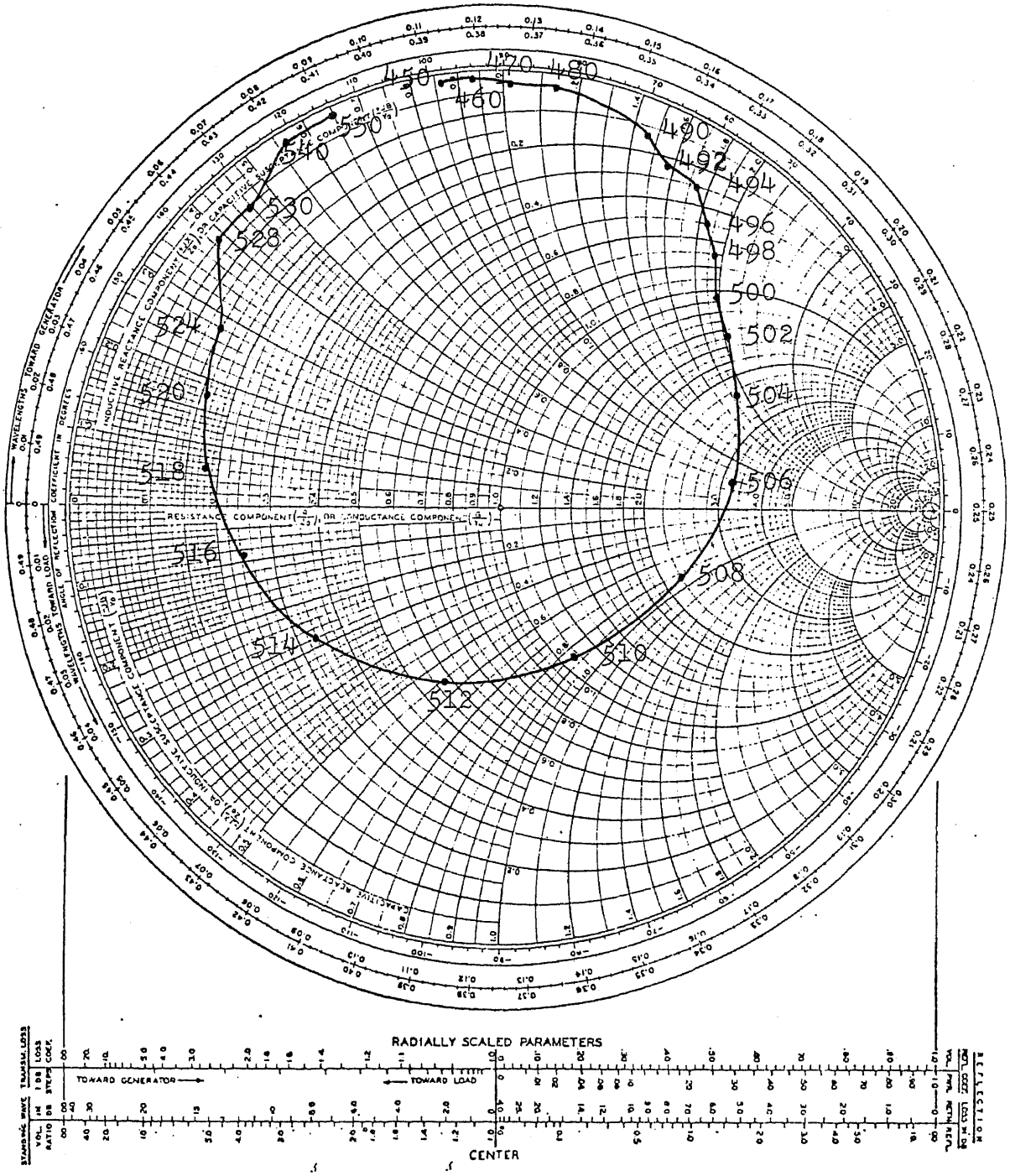

Fig. 2.4.1.a. Reflection coefficients of YIG tuning element for signals from 450 to 550 MHZ and electromagnet current I of 25 mA.

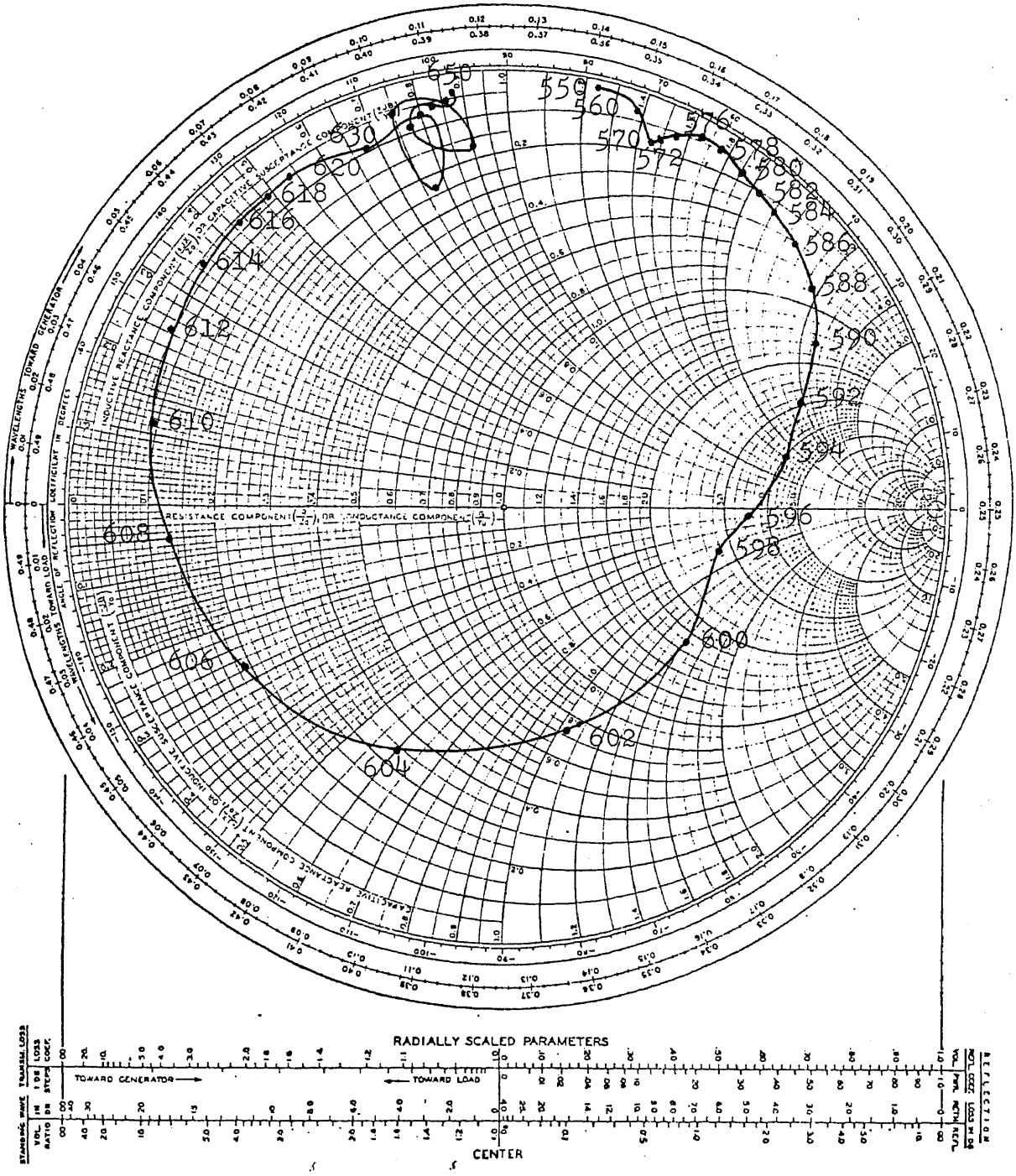

Fig. 2.4.1.b. Reflection coefficients of YIG tuning element for signals from 550 to 650 MHZ and electromagnet current I of 32.5 mA.

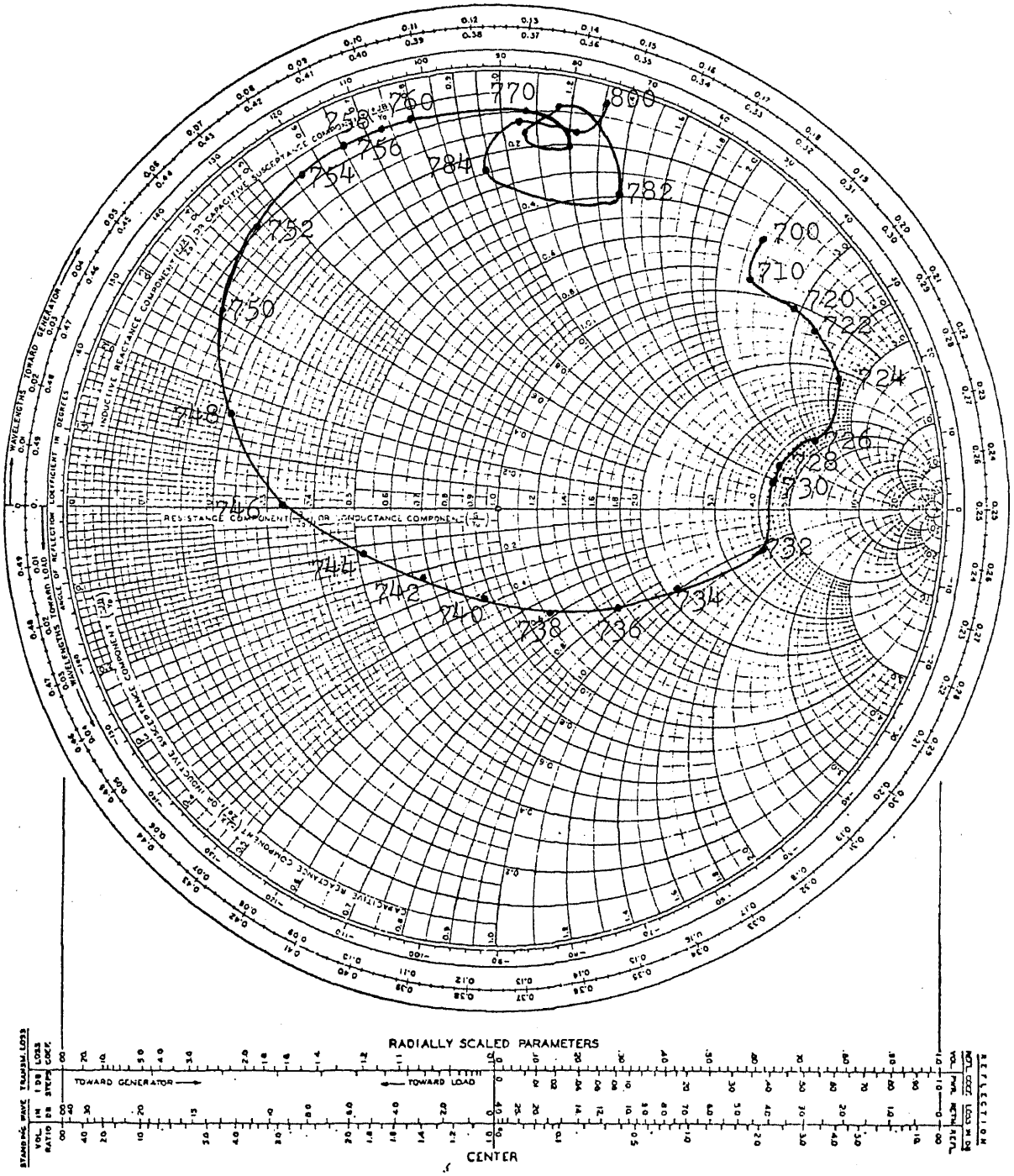

Fig. 2.4.1.c. Reflection coefficients of YIG tuning element for signals from 700 to 800 MHZ and electromagnet current I of 41 mA.

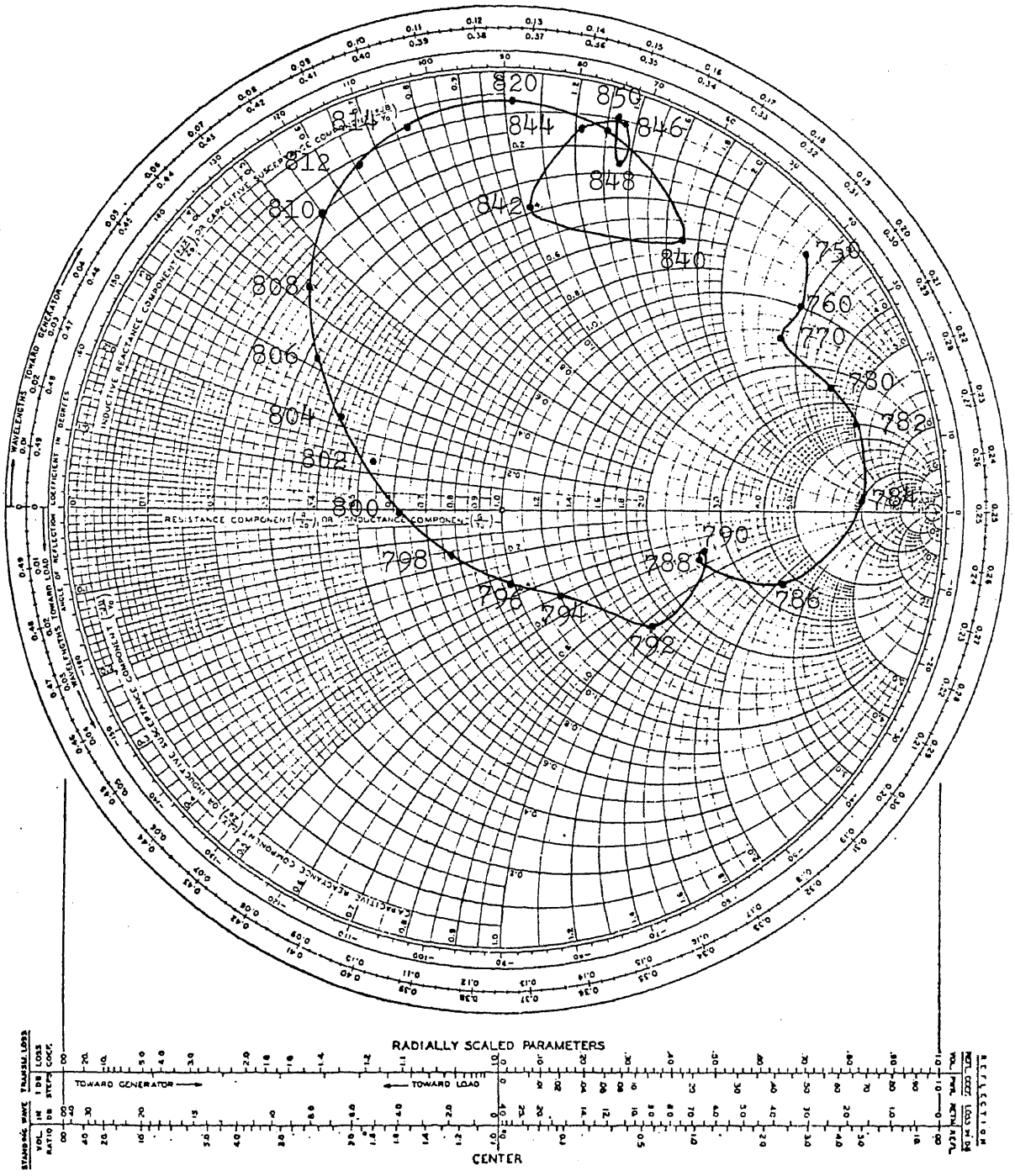

Fig. 2.4.1.d. Reflection coefficients of YIG tuning element for signals from 750 to 850 MHZ and electromagnet current I of 46 mA.

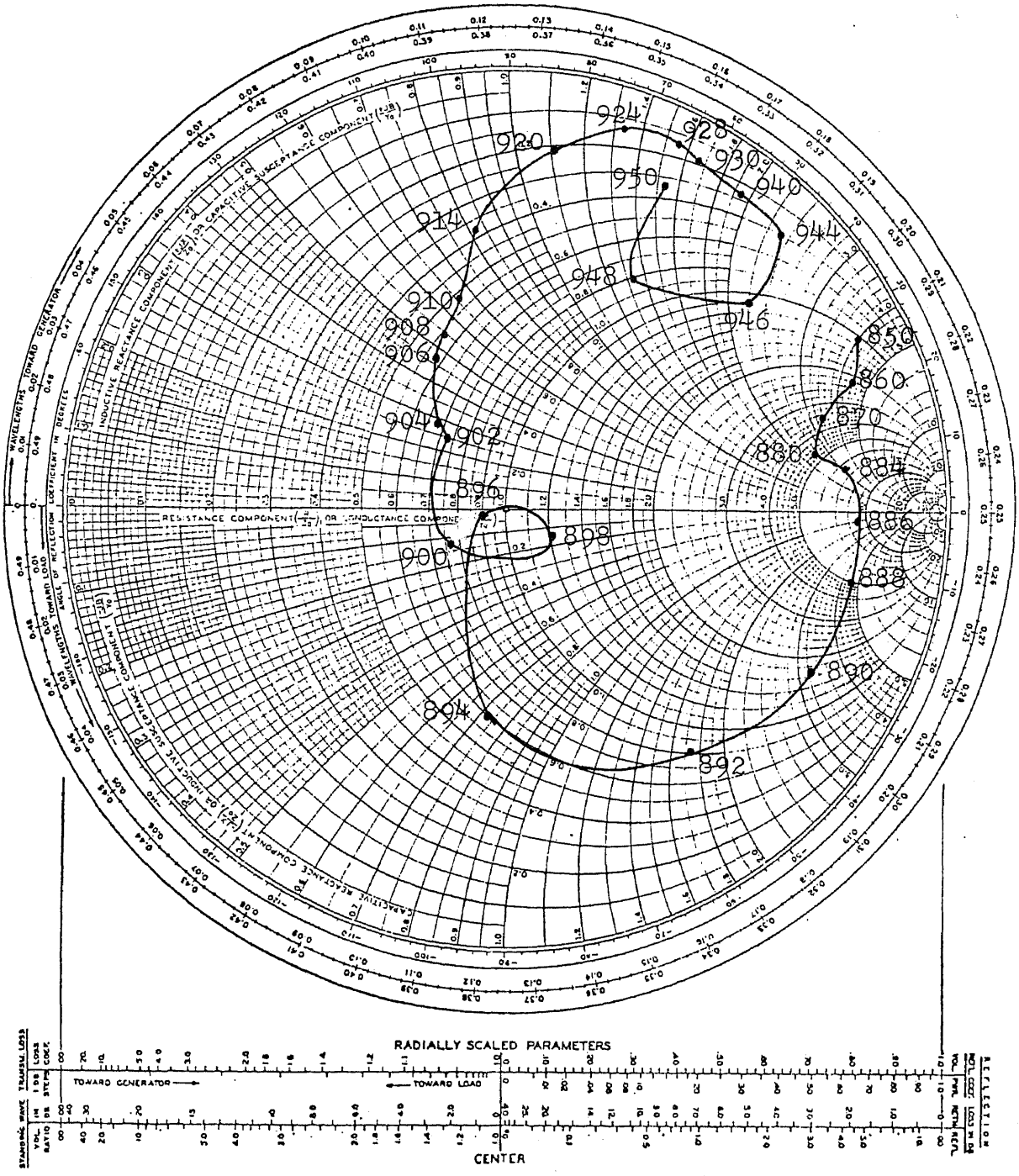

Fig. 2.4.1.e. Reflection coefficients of YIG tuning element for signals from 850 to 950 MHZ and electromagnet current I of 52 mA.

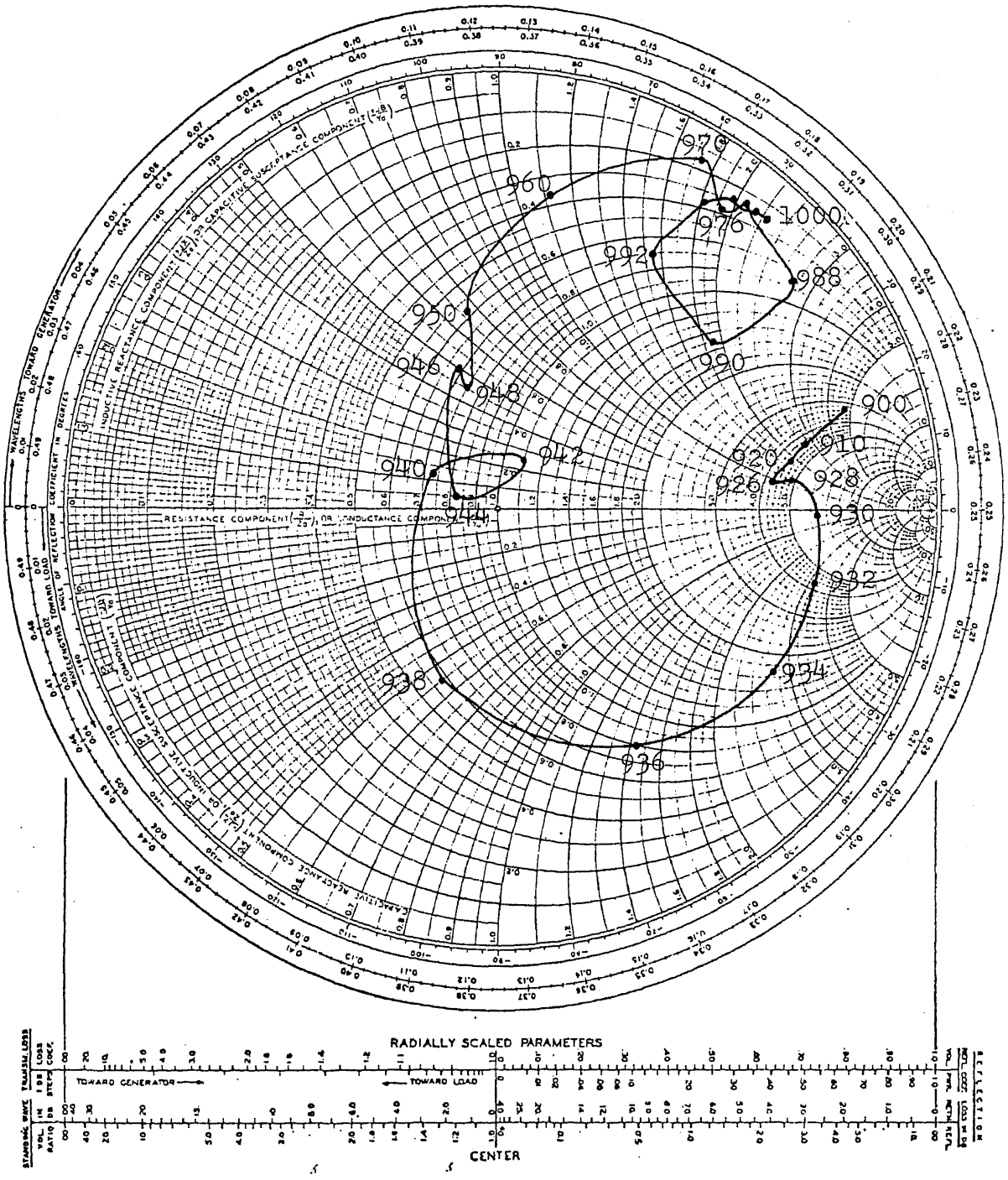

Fig. 2.4.1.f. Reflection coefficients of YIG tuning element for signals from 900 to 1000 MHZ and electromagnet current I of 55 mA.

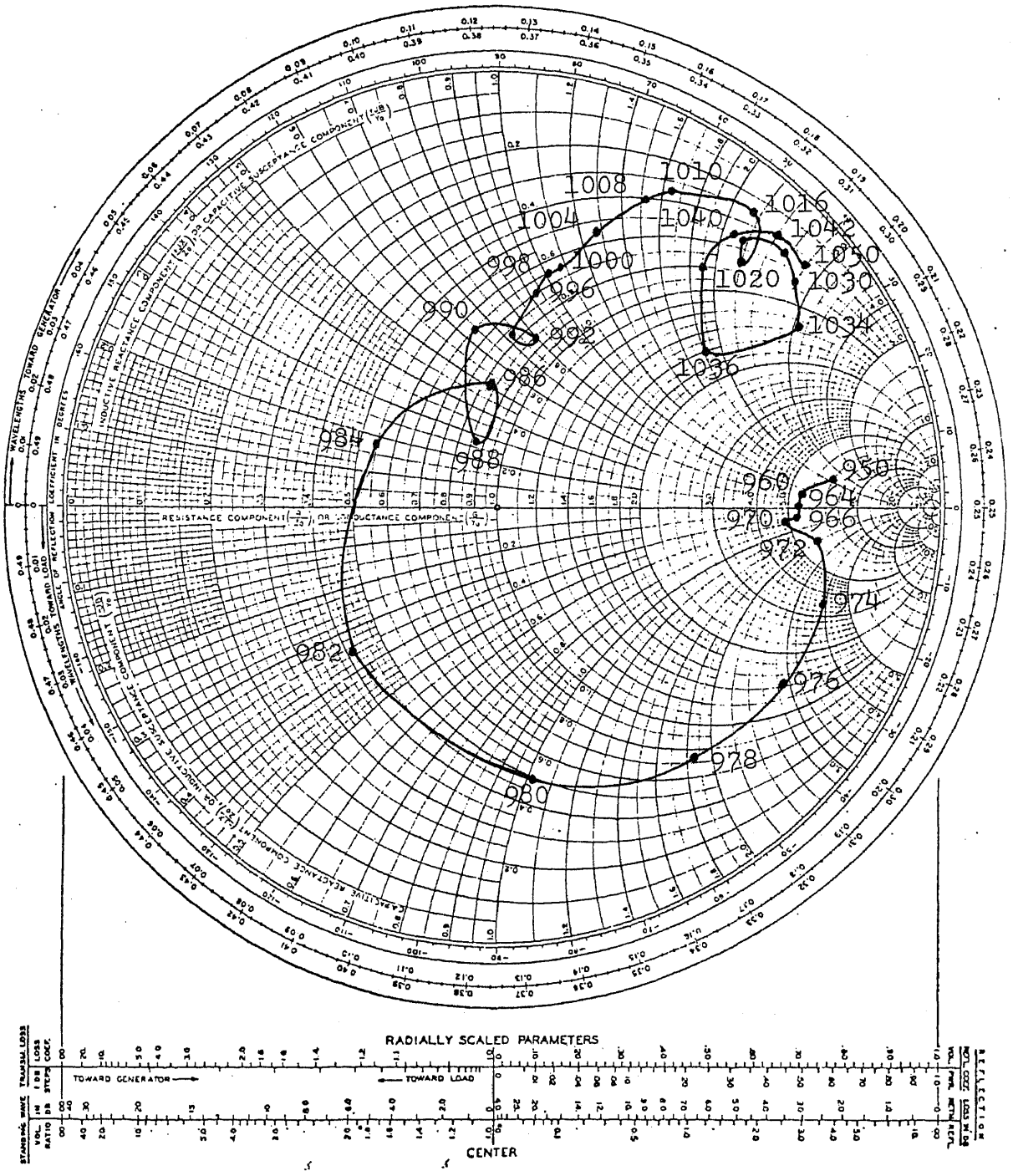

Fig. 2.4.1.g. Reflection coefficients of YIG tuning element for signals from 950 to 1050 MHZ and electromagnet current I of 58 mA.

CHAPTER 3

MAGNETIC STRUCTURE

3.1. The Electromagnet

The electromagnet used to provide the biasing dc magnetic field for the YIG sphere is shown in Fig. 3.1.1.

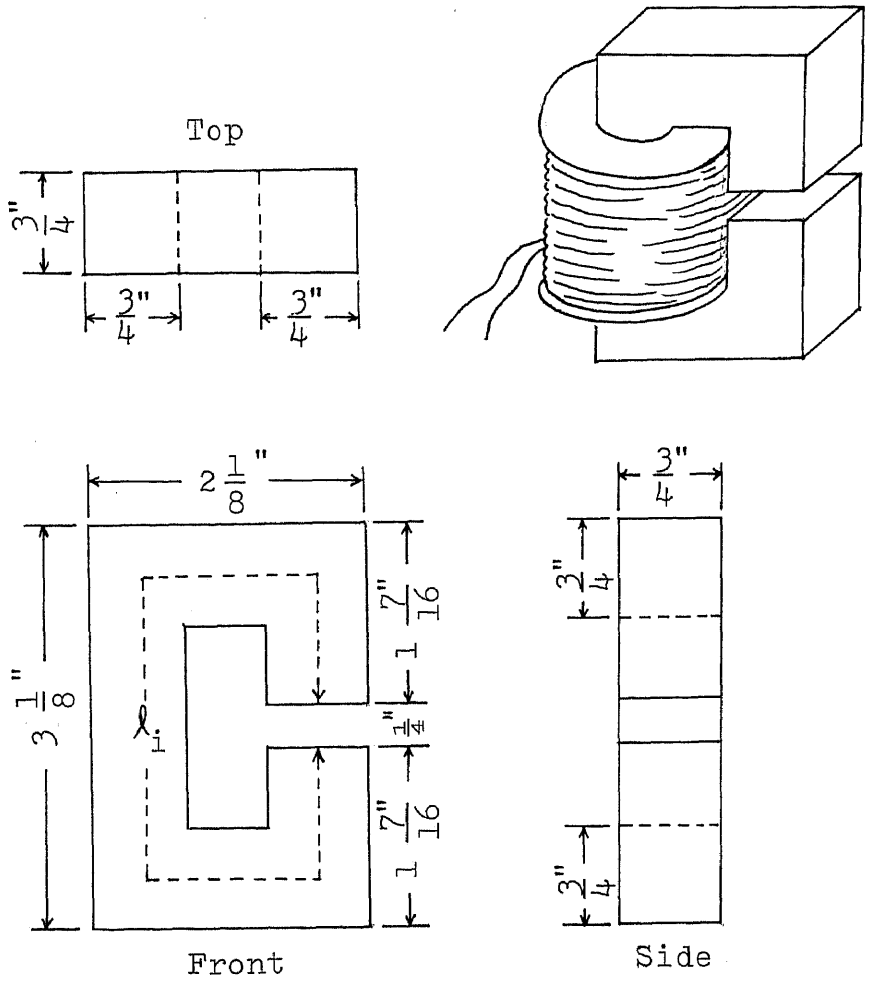

Fig. 3.1.1. Magnetic structure and dimensions of the iron core.

The magnetic structure was designed to satisfy the following conditions:

(1) large pole faces to provide a uniform field over the YIG sphere,
(2) sufficiently wide air gap to contain the YIG and coupling loop,
(3) to provide a magnetic field variable from 150 to 350 gausses in the air gap.

The choice of this particular structure is based on the simplicity of its construction. The core of the electromagnet is made of two sections of L-shaped iron blocks held together with machine screws. A (1/4)" air gap in one leg of the core is designed to be occupied by the mounting and coupling structure of the YIG sphere.

The coil is wound with 5,000 turns of #30 wire and the total resistance of the windings is approximately 200 ohms. Therefore, power dissipation of approximately 0.7 watts at 60 mA can be expected.

3.2. Magnetic-Circuit Calculations

Magnetic-circuit calculations take into account the effects of fringing and leakage fluxes. Thus, if the cross-sectional dimensions of the core are the same on both faces of the gap, a correction factor of 2δ,

where δ is the length of the actual air gap, would be applied in computing the equivalent air-gap area. Such corrections account for the increase in flux density in the iron as a result of fringing and leakage fluxes [20]. Thus, the effective cross-sectional area of the gap is given by

$$A_a = (a + 2\delta)(b + 2\delta), \qquad (3.2.1)$$

where

A_a = effective area of air gap

δ = length of actual air-gap

a and b are the cross-sectional dimensions of the actual core faces.

Assuming the flux density within the equivalent gap is uniform, then the total flux is

$$\phi_a = B_a A_a, \qquad (3.2.2)$$

where

ϕ_a = total flux in air gap

B_a = flux density in air gap.

The magnetomotive force required of the coil to establish the magnetizing force H_a in the air gap is given by

$$F = H_a \ell_a + H_i \ell_i, \qquad (3.2.3)$$

where

F = magnetomotive force for the circuit = NI

H_a = magnetizing force in air gap

H_i = magnetizing force in iron

ℓ_a = length of air gap

ℓ_i = length of mean path in iron

N = number of turns in coil

I = current through the coil.

Since the total flux in the air gap is approximately equal to the flux in the iron ϕ_i, the flux density in the iron can be derived from

$$\phi_i = \phi_a . \qquad (3.2.4)$$

Thus,

$$B_i = \frac{B_a A_a}{A_i} , \qquad (3.2.5)$$

where

B_i = flux density in iron core

A_i = actual core area = a x b

B_a and A_a are as previously defined.

The magnetizing force in iron, H_i, can be determined from intrinsic magnetization curves {20}. Substituting the values read from the curves and those

shown in Fig. 3.1.1 into equation (3.2.3) and applying the unit conversion formulas

$$H\ (Oe) = B\ (gauss) \tag{3.2.6}$$

$$H\ (amp\text{-}turns/in) = \frac{2.54}{0.4\pi} \times H\ (Oe) \tag{3.2.7}$$

$$H\ (amp\text{-}turns/in) = 313 \times B\ (Kilolines/sq.\ in.) \tag{3.2.8}$$

to the equations above, the values listed in Table I are obtained.

TABLE I. Magnetizing Forces and Currents

H_a	B_i	H_i	I
200	3.58	5	27.46
250	4.48	5.5	33.24
300	5.38	6	39.02
350	6.28	6.5	44.80

where

H_a = magnetizing force in the air gap in oersteds

B_i = flux density of iron in kilolines/sq. in.

H_i = magnetizing force in the iron in amp-turns/in. (read from magnetization curve)

I = current in mA through the windings of the electromagnet.

The results from the tabulation are plotted in Fig. 3.2.1. In the same figure, the measured data of the actual magnetic circuit is also shown.

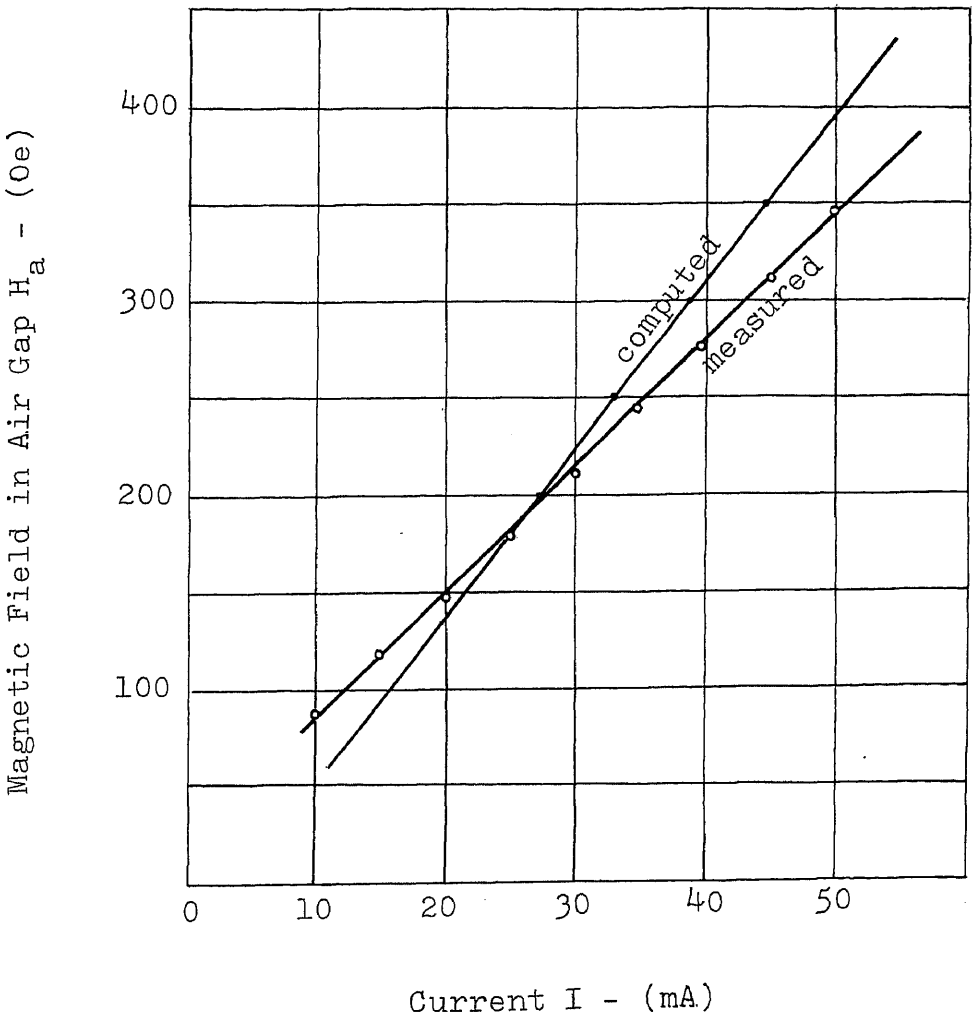

Fig. 3.2.1. Magnetic field in the air gap versus current through the windings of the electromagnet.

The discrepancies between computed values and measured data are due to the approximations involved in the calculations. Furthermore, the values of H_i are not obtained from the actual magnetization curve of the core material. However, the measured data indicate that the magnetizing force in the air gap varies linearly with the current through the windings of the electromagnet.

CHAPTER 4

OSCILLATOR DESIGN

A technique for designing YIG-tuned transistor oscillators, tunable over the range of frequencies from 500 to 950 MHZ, is presented. The analysis of the oscillator circuit is based on reflection coefficients measured at network terminals of various design stages. Smith Charts and signal flow graph analysis are used to simplify network calculations.

The choice of a transistor for the oscillator circuit depends on whether the condition for oscillation can be satisfied. This requirement is met if measured reflection coefficients of the transistor have magnitudes greater than unity over the specified range of frequencies. Otherwise, the transistor must be properly terminated or external feedback must be provided to derive such condition.

When an RCA 2N2857 transistor connected in common-base configuration has its emitter lead terminated in 50 ohms, reflection coefficients measured at the collector have magnitudes greater than unity. Therefore, this transistor is chosen for the oscillator circuit. The necessary condition for oscillation results when the transistor is operated at a quiescent

point of V_{ce} = 6 volts and I_c = 12 mA. Detailed analyses of the oscillator circuit are covered in subsequent sections.

4.1. DC Analysis

The dc analysis of the transistor circuit is based on Fig. 4.1.1.

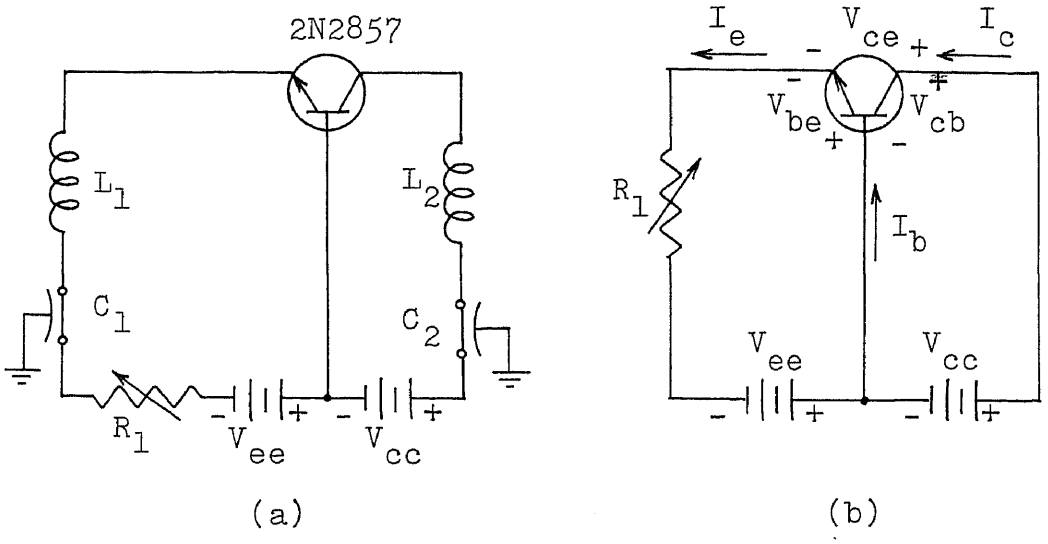

Fig. 4.1.1. Transistor circuit for dc analysis. (a) dc biasing circuit, (b) simplified dc circuit.

The transistor circuit is to be designed for the following quiescent operating point:

$$V_{ce} = 6 \text{ volts}$$

$$I_c = 12 \text{ mA.}$$

In Fig. 4.1.1(a), L_1 and L_2 are radio-frequency chokes; C_1 and C_2 are feed-thru capacitors. Since their dc resistances are negligible, their effects are ignored in the dc analysis of the circuit.

From the simplified circuit shown in Fig. 4.1.1(b), the following equations can be obtained:

$$V_{ee} = V_{be} + I_e R_1 \tag{4.1.1}$$

$$V_{cc} = V_{cb} \tag{4.1.2}$$

$$V_{cc} = V_{ce} + I_e R_1 - V_{ee} \tag{4.1.3}$$

$$= V_{ce} - V_{be} \ .$$

In order to stabilize the quiescent operating point, resistor R_1 is connected in series with the emitter of the transistor. To examine stability, let

$$I_e = I_b + I_c \tag{4.1.4}$$

$$I_c = \beta I_b + I_{ceo}, \tag{4.1.5}$$

where I_{ceo} is the current flowing across the reverse-biased collector junction as a result of thermal generation of carriers near the junction {3}.

Substituting equations (4.1.4) and (4.1.5) into equation (4.1.1), and solving for I_c gives

$$I_c = \frac{\beta (V_{ee} - V_{be})}{(1 + \beta) R_1} + \frac{1}{(1 + \beta)} I_{ceo} . \qquad (4.1.6)$$

If I_{ceo} changes to $(I_{ceo} + \Delta I_{ceo})$, I_c also changes and is given by

$$I_c + \Delta I_c = \frac{\beta (V_{ee} - V_{be})}{(1 + \beta) R_1} + \frac{1}{(1 + \beta)} (I_{ceo} + \Delta I_{ceo}) \qquad (4.1.7)$$

Subtracting equation (4.1.6) from (4.1.7) yields

$$\Delta I_c = \frac{1}{(1 + \beta)} \Delta I_{ceo} \qquad (4.1.8)$$

The stability factor is then defined by

$$S = \frac{\Delta I_c}{\Delta I_{ceo}} = \frac{1}{(1 + \beta)} \qquad (4.1.9)$$

Notice that if $\beta >> 1$, then equations (4.1.6) and (4.1.9) give

$$I_c \approx \frac{V_{ee} - V_{be}}{R_1} \qquad (4.1.6.a)$$

$$S \approx \frac{1}{\beta} \approx 0 \qquad (4.1.9.a)$$

Calculations:

If V_{ee} were chosen such that $V_{ee} >> V_{be}$, then equation (4.1.6.a) for I_c becomes independent of the transistor parameters. Since $V_{be} = 0.7$ volts, V_{ee} is chosen to be 7 volts. Thus, for $V_{ce} = 6$ volts and $I_c = 12$ mA,

$$R_1 = \frac{V_{ee} - V_{be}}{I_c} = \frac{7 - 0.7}{12 \text{ mA}} = 0.525 \text{ K}\Omega$$

$$V_{cc} = V_{ce} - V_{be} = 6 - 0.7 = 5.3 \text{ volts}$$

The approximations made above for I_c and S hold because the measured value of β for the 2N2857 transistor is approximately 100, which is much larger than 1.

To summarize, the operating levels and components are

$V_{ce} = 6$ volts, $\quad I_c = 12$ mA

$V_{cc} = 5.3$ volts

$V_{ee} = 7$ volts

$R_1 = 1$ KΩ pot (set at = 525Ω).

4.2. AC Analysis

As shown in Fig. 2.2.2, a single YIG coupled loop behaves like a parallel LC resonant circuit. Therefore, it can be used as a frequency determining network for

the oscillator. Figures 2.4.1a through 2.4.1g show the characterization of the YIG resonator by reflection coefficients measured at terminals of the loop around the YIG sphere.

The transistor can also be characterized by reflection and transmission coefficients, i.e., s(scattering)-parameters. Scattering-parameters relate the waves reflected from a two-port network to those waves incident upon the network. These relationships can be summarized by two sets of equations {2}:

$$b_1 = S_{11}a_1 + S_{12}a_2 \tag{4.2.1}$$

$$b_2 = S_{21}a_1 + S_{22}a_2, \tag{4.2.2}$$

where a_1, a_2, b_1 and b_2 are defined by

$$a_1 = \frac{E_{1(\text{incident})}}{\sqrt{Z_o}} = \frac{E_{i1}}{\sqrt{Z_o}} \tag{4.2.3}$$

$$a_2 = \frac{E_{2(\text{incident})}}{\sqrt{Z_o}} = \frac{E_{i2}}{\sqrt{Z_o}} \tag{4.2.4}$$

$$b_1 = \frac{E_{1(\text{reflected})}}{\sqrt{Z_o}} = \frac{E_{r1}}{\sqrt{Z_o}} \tag{4.2.5}$$

$$b_2 = \frac{E_{2(\text{reflected})}}{\sqrt{Z_o}} = \frac{E_{r2}}{\sqrt{Z_o}} \tag{4.2.6}$$

E_{i1} and E_{i2} are voltage waves incident upon terminals 1 and 2 of the network, respectively; and E_{r1} and E_{r2} are voltage waves reflected from terminals 1 and 2 of the network, respectively. Z_o is the characteristic impedance of the transmission line in ohms. Therefore, a_1^2, a_2^2, b_1^2 and b_2^2 will have dimensions of power. The scattering-parameters are defined by:

$$S_{11} = \left.\frac{b_1}{a_1}\right|_{a_2 = 0}$$ = input reflection coefficient with the output port terminated by a matched load ($Z_L = Z_o$),

$$S_{22} = \left.\frac{b_2}{a_2}\right|_{a_1 = 0}$$ = output reflection coefficient with the input port terminated by a matched load ($Z_s = Z_o$ and $V_s = 0$),

$$S_{21} = \left.\frac{b_2}{a_1}\right|_{a_2 = 0}$$ = forward transmission coefficient with the output port terminated in a matched load,

$$S_{12} = \left.\frac{b_1}{a_2}\right|_{a_1 = 0}$$ = reverse transmission coefficient with the input port terminated in a matched load.

Scattering-parameters for 2N2857 transistor, measured with an HP 8745A S-Parameter Test Set, are

plotted in Figure 4.2.1. The characteristic impedance of the reference system is 50 ohms. Test signal levels of -15 dBm and -35dBm are applied to obtain two sets of measured parameters in the frequency range from 500 to 1000 MHZ. The normalized input and output impedances can be read directly as [z] = Re(z) + jIm(z) from the curves of S_{11} and S_{22}, respectively. Actual impedances are then obtained by multiplying the normalized values by 50.

Since the magnitude of S_{22} is greater than one, $(1/S_{22})$ is plotted instead. A normalized complex impedance [z'] can be read as before. The actual normalized impedance [z] , however, is the negative of [z']. Actual impedance is again obtained by multiplying the normalized value by 50.

Using signal flow graph techniques {2}, the transistor can be represented by the diagram shown in Fig. 4.2.2, in which the S-parameters form the branches while the incident and reflected waves form the nodes. In this representation, branches originate from the independent variable nodes (a_1 and a_2) and enter the dependent nodes (b_1 and b_2).

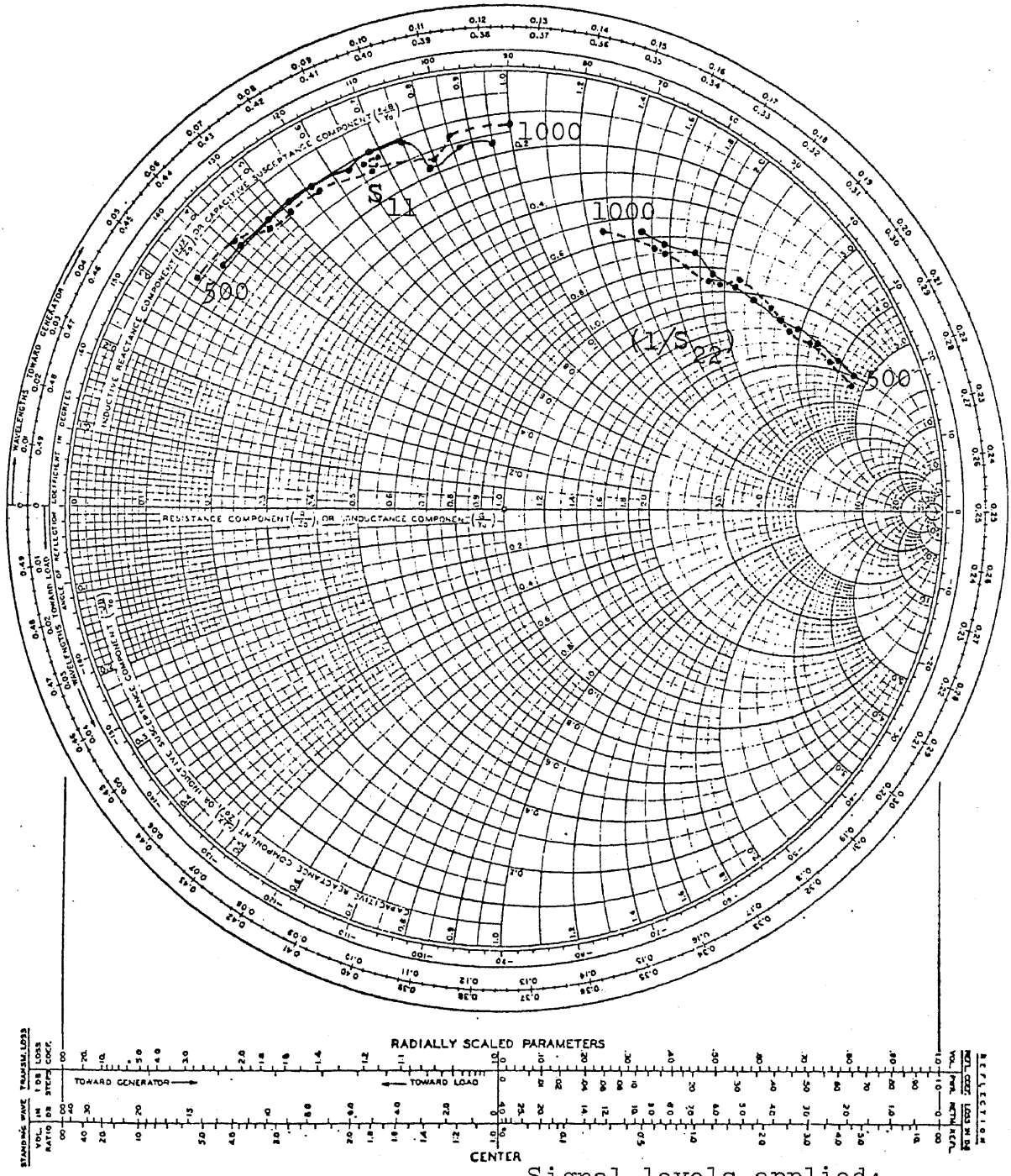

Signal levels applied:
——— -15 dBm
----- -35 dBm

Fig. 4.2.1.a. S_{11} and $(1/S_{22})$ parameters, from 500 to 1000 MHZ at 50 MHZ intervals, of 2N2857 transistor in common-base configuration.

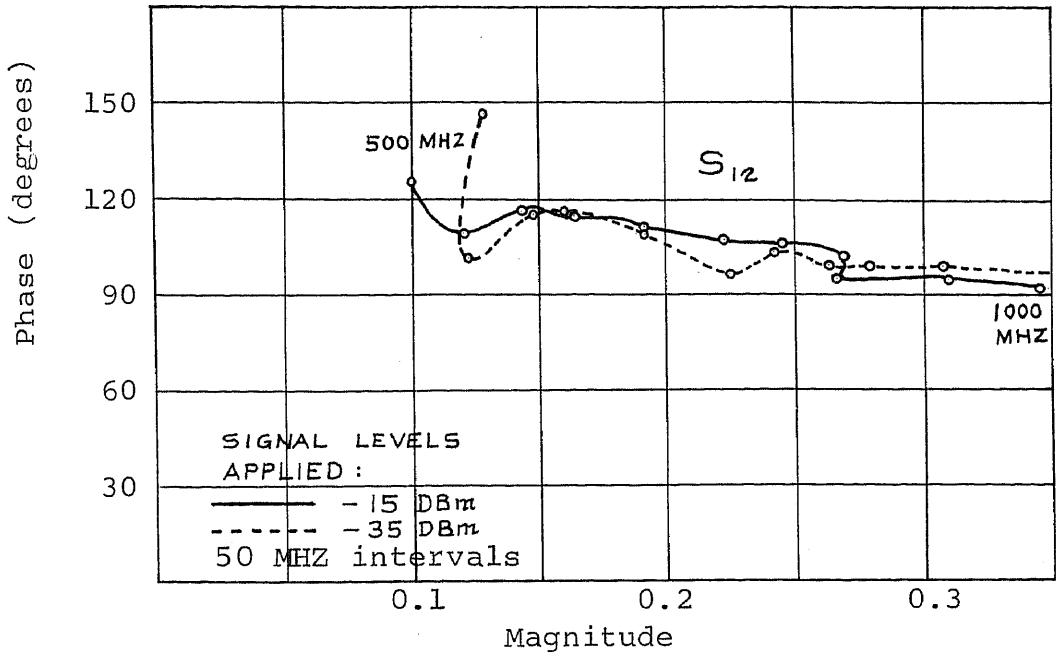

Fig. 4.2.1.b. S_{12} parameter, from 500 to 1000 MHZ, of 2N2857 transistor in common-base configuration.

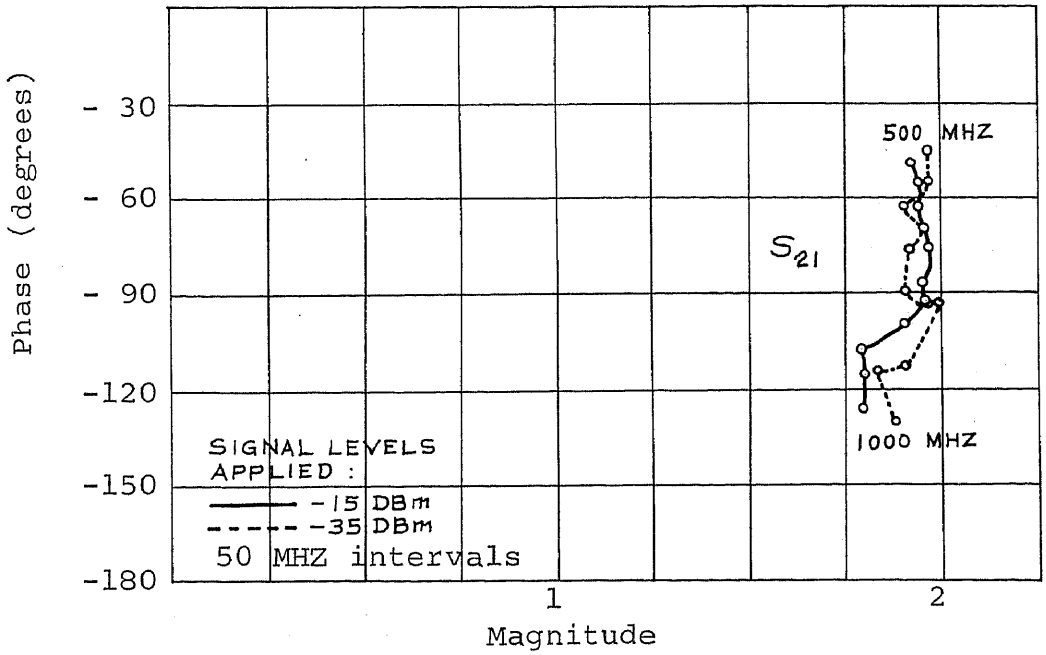

Fig. 4.2.1.c. S_{21} parameter, from 500 to 1000 MHZ, of 2N2857 transistor in common-base configuration.

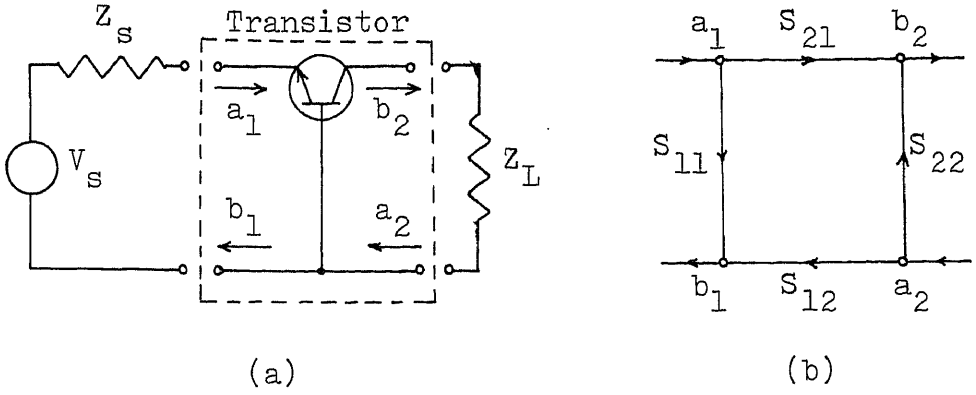

Fig. 4.2.2. (a) transistor, (b) flow graph representation.

The signal flow graph representation of a load connected at the output port is simply Γ_L, the complex reflection coefficient of the load, as shown in Fig. 4.2.3.

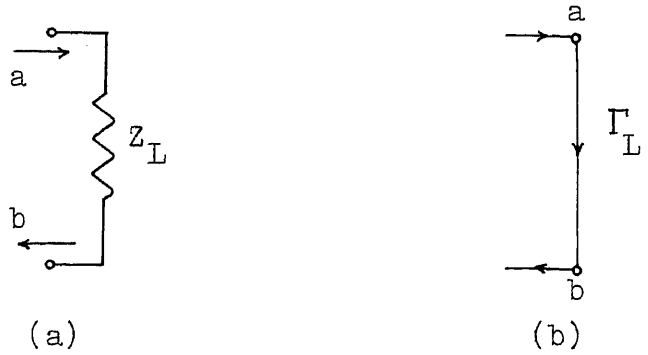

$$\Gamma_L = \frac{b}{a} = \frac{Z_L - Z_o}{Z_L + Z_o} \qquad (4.2.7)$$

Fig. 4.2.3. (a) load Z_L, (b) flow graph representation.

The modified reflection coefficient, S'_{11}, with the output port terminated in any arbitrary load and $Z_s = Z_o$ can be determined from Fig. 4.2.4.

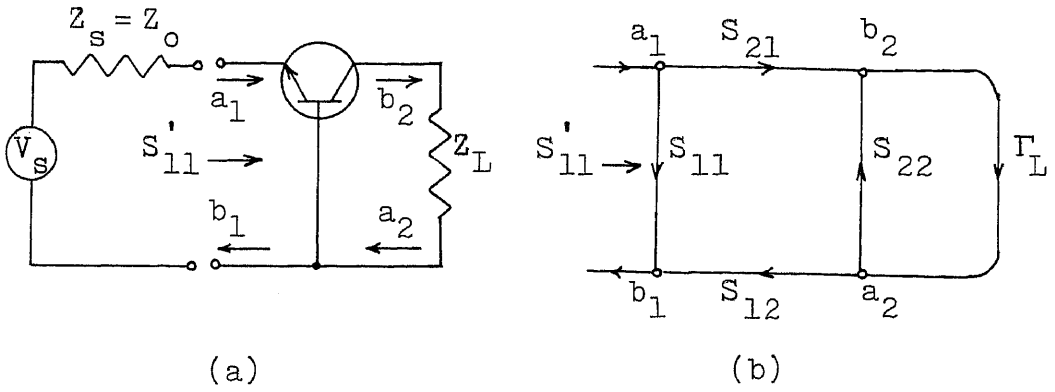

Fig. 4.2.4. (a) Transistor with output termination arbitrary and $Z_s = Z_o$, (b) flow graph of (a).

Applying Mason's rule [2] to Fig. 4.2.4(b), S'_{11} becomes

$$S'_{11} = \frac{b_1}{a_1} = \frac{S_{11}(1 - S_{22}\Gamma_L) + S_{21}\Gamma_L S_{12}}{1 - S_{22}\Gamma_L}$$

or

$$S'_{11} = S_{11} + \frac{S_{12}S_{21}\Gamma_L}{1 - S_{22}\Gamma_L} . \qquad (4.2.8)$$

With certain transistors S'_{11} can be made greater than unity by introducing external feedback or by proper choice of Γ_L. This means that the real part of the

input impedance of the network will be negative. In this case the network can be used for oscillator circuits {2}.

The stability of the circuit also depends upon the source impedance. A source with some internal voltage V_s and internal impedance Z_s can be represented by the diagrams in Fig. 4.2.5.

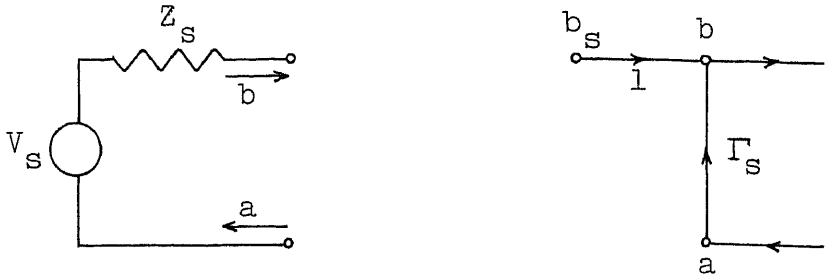

(a) (b)

Fig. 4.2.5. (a) Source representation, (b) flow graph of source.

Γ_s is the source reflection coefficient given by

$$\Gamma_s = \frac{Z_s - Z_o}{Z_s + Z_o} \qquad (4.2.9)$$

and b_s, the wave from the source, is given by

$$b_s = \frac{V_s \sqrt{Z_o}}{Z_s + Z_o} . \qquad (4.2.10)$$

The magnitude of b_s squared, therefore, has the dimensions of power, which conforms with the definitions of incident and reflected waves given previously.

By connecting the source to the input terminals of the network, Fig. 4.2.6 is obtained.

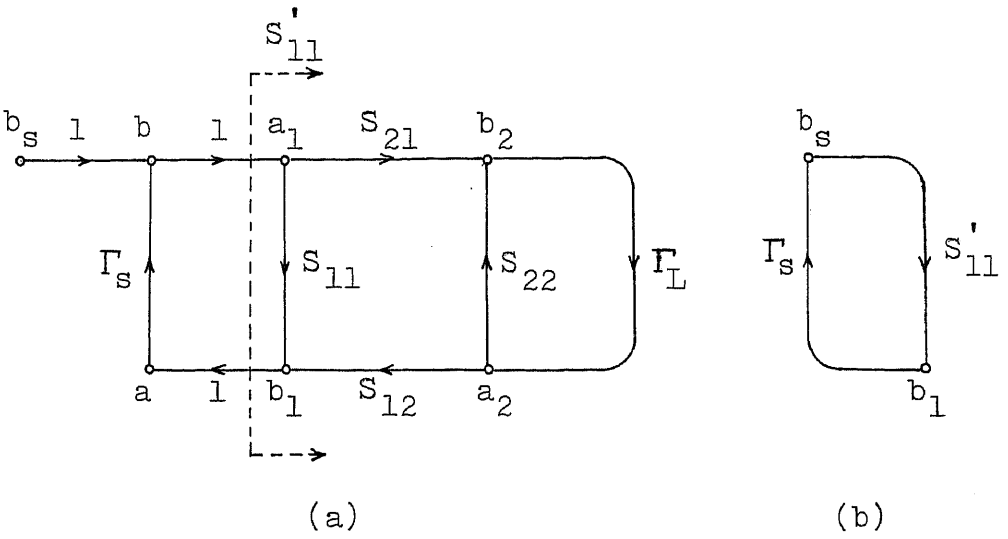

Fig. 4.2.6. (a) Flow graph of network with source and load connected, (b) simplified diagram.

Based on the simplified diagram shown in Fig. 4.2.6(b), the ratio of the reflected wave b_1 to the input wave b_s can be determined by applying Mason's rule again. Thus

$$\frac{b_1}{b_s} = \frac{S'_{11}}{1 - \Gamma_s S'_{11}} \qquad (4.2.11)$$

At a frequency such that

$$\Gamma_s S'_{11} = 1, \qquad (4.2.12)$$

the circuit becomes unstable and will oscillate. However, if

$$\left|S'_{11}\right| < \left|\frac{1}{\Gamma_s}\right|,$$

the circuit will cease to oscillate {2}.

If the source were replaced by a tuned circuit, Γ_s becomes Γ_m, where Γ_m is the reflection coefficient of the tuned circuit. In order for the circuit to oscillate at a certain frequency, the tuned circuit must be adjusted so that Γ_m satisfies the equation

$$\Gamma_m S'_{11} = 1 \qquad (4.2.12.a)$$

at that frequency.

If equation (4.2.12.a) is not satisfied by the transistor and tuned circuit, an impedance transforming network can be inserted between them to satisfy the condition for oscillation. The design of such a network is discussed in the next section.

4.3. Impedance Transforming Network

The condition for oscillation can be achieved by means of an impedance transforming network connected between the YIG tuning element and the transistor. This network, shown in Fig. 4.3.1, consists of a shunt capacitance C_3 and a length of transmission line making up the series inductance L_3. The approximate length of this line can be determined from the equation for the self-inductance of straight round wires[22]

$$L_o = 0.00508\,\ell\,(2.303\,\log_{10}\frac{4\ell}{d} - 1)\ \text{microhenrys}, \tag{4.3.1}$$

where

L_o = self-inductance of straight round wire

ℓ = length of wire in inches

d = diameter of wire in inches.

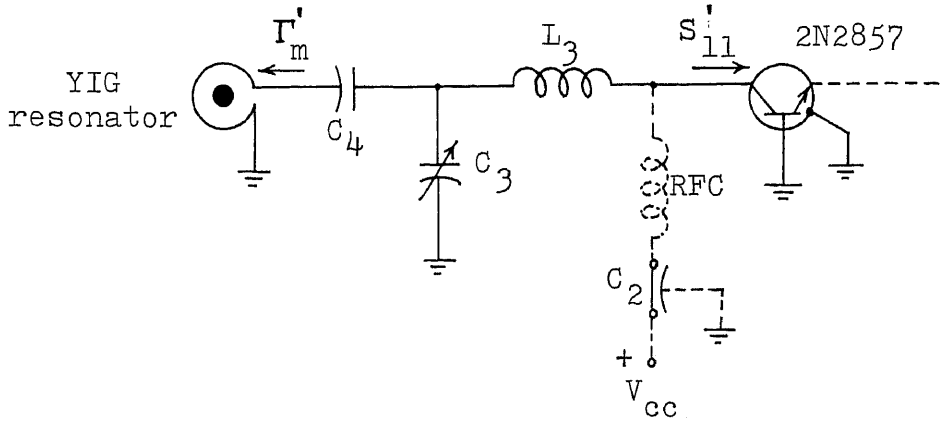

Fig. 4.3.1. Impedance transforming network.

C_4 is a dc blocking capacitor.

The performance of this network for various frequencies of oscillation is shown in Fig. 4.3.2. Portions of curves of reflection coefficients of the YIG tuning element (from Fig. 2.4.1) are repeated in this figure. These diagrams show the transformation between the impedance at the output of the YIG tuning element, represented by Γ_m', and the input of the transistor, represented by S_{11}', such that oscillating conditions can be satisfied.

Since the collector terminal of transistor 2N2857 has a negative real part, as shown by a reflection coefficient of magnitude greater than unity, it can be used at the input terminal with no external feedback. Thus S_{11}' is equal to S_{22} of transistor 2N2857. In order for the circuit to oscillate, Γ_m must satisfy equation (4.2.12.a). Therefore, any point B lying on the line $|\Gamma_m| \geq |(1/S_{22})|$ and phase Γ_m = phase $(1/S_{22})$ will satisfy this requirement. Notice that the curve of $(1/S_{22})$ is also plotted in Fig. 4.3.2 for reference. It can be seen from the same figure that due to the shunt capacitance, the transformation from the YIG tuning element follows a constant conductance circle by the amount ωC_3 until point A is reached. From point A the transformation follows a constant resistance

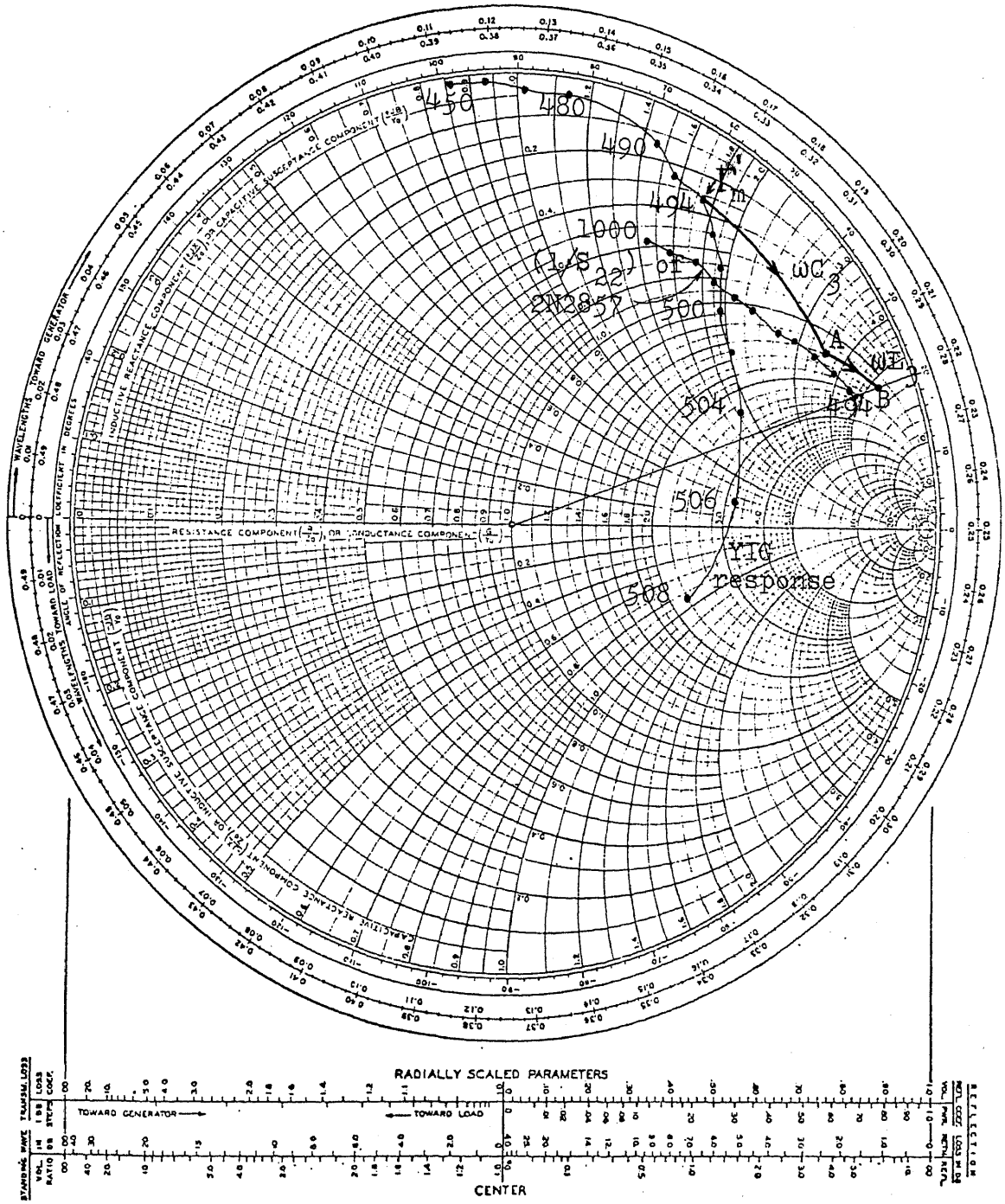

Fig. 4.3.2.a. Smith chart diagram showing transformation which satisfies condition for oscillation at 494 MHZ and electromagnet current I of 25 mA.

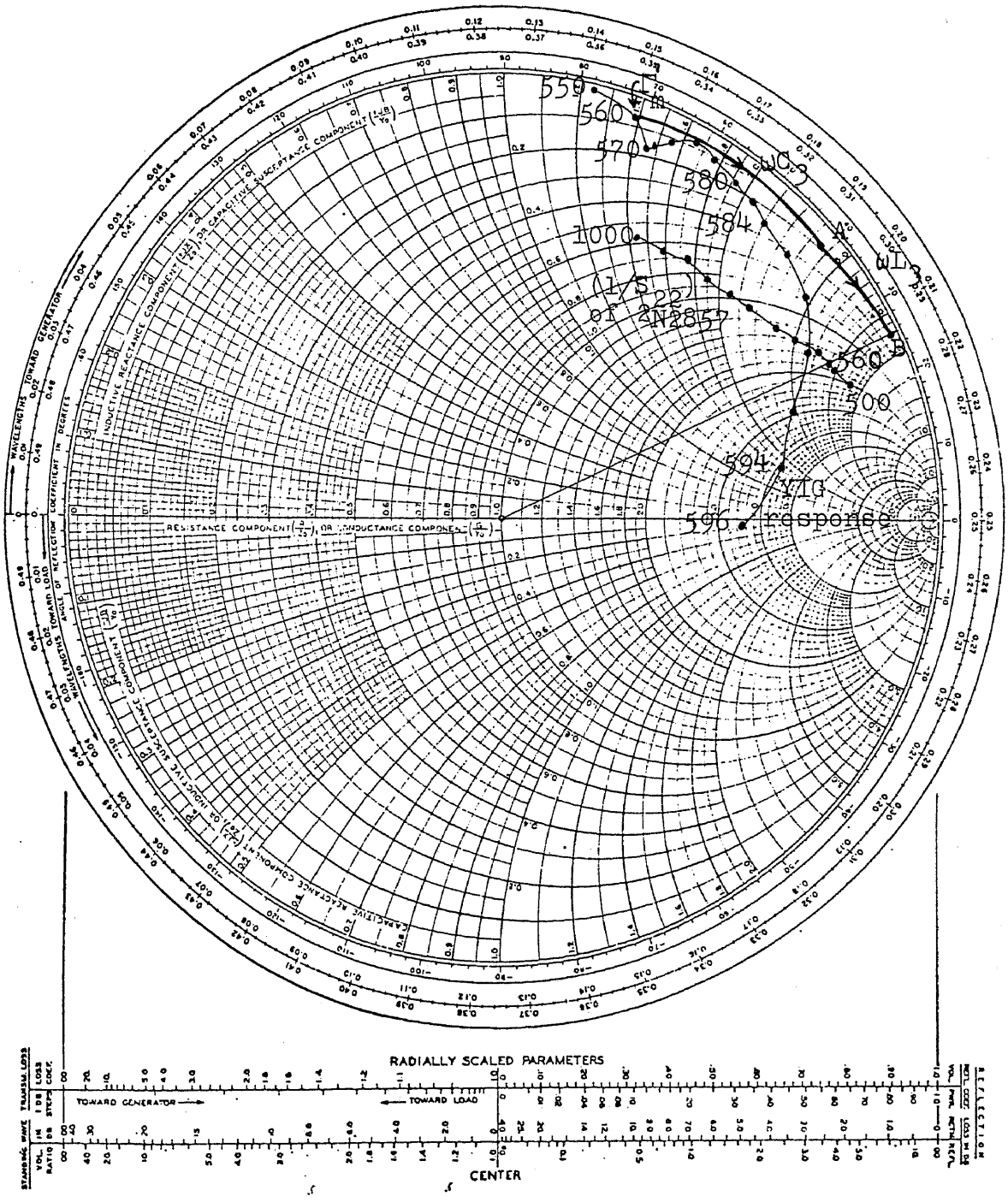

Fig. 4.3.2.b. Smith chart diagram showing transformation which satisfies condition for oscillation at 560 MHZ and electromagnet current I of 32.5 mA.

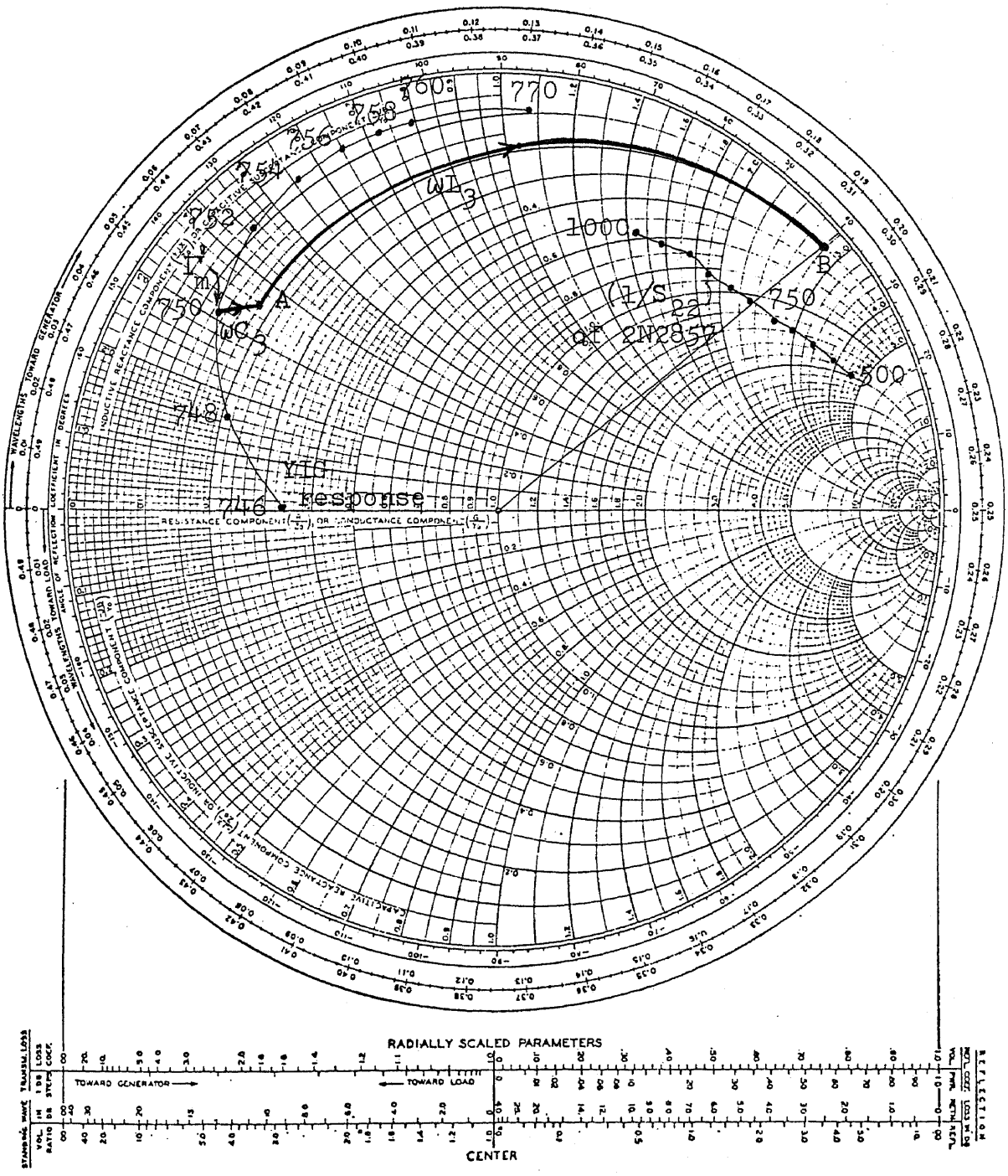

Fig. 4.3.2.c. Smith chart diagram showing transformation which satisfies condition for oscillation at 750 MHZ and electromagnet current I of 41 mA.

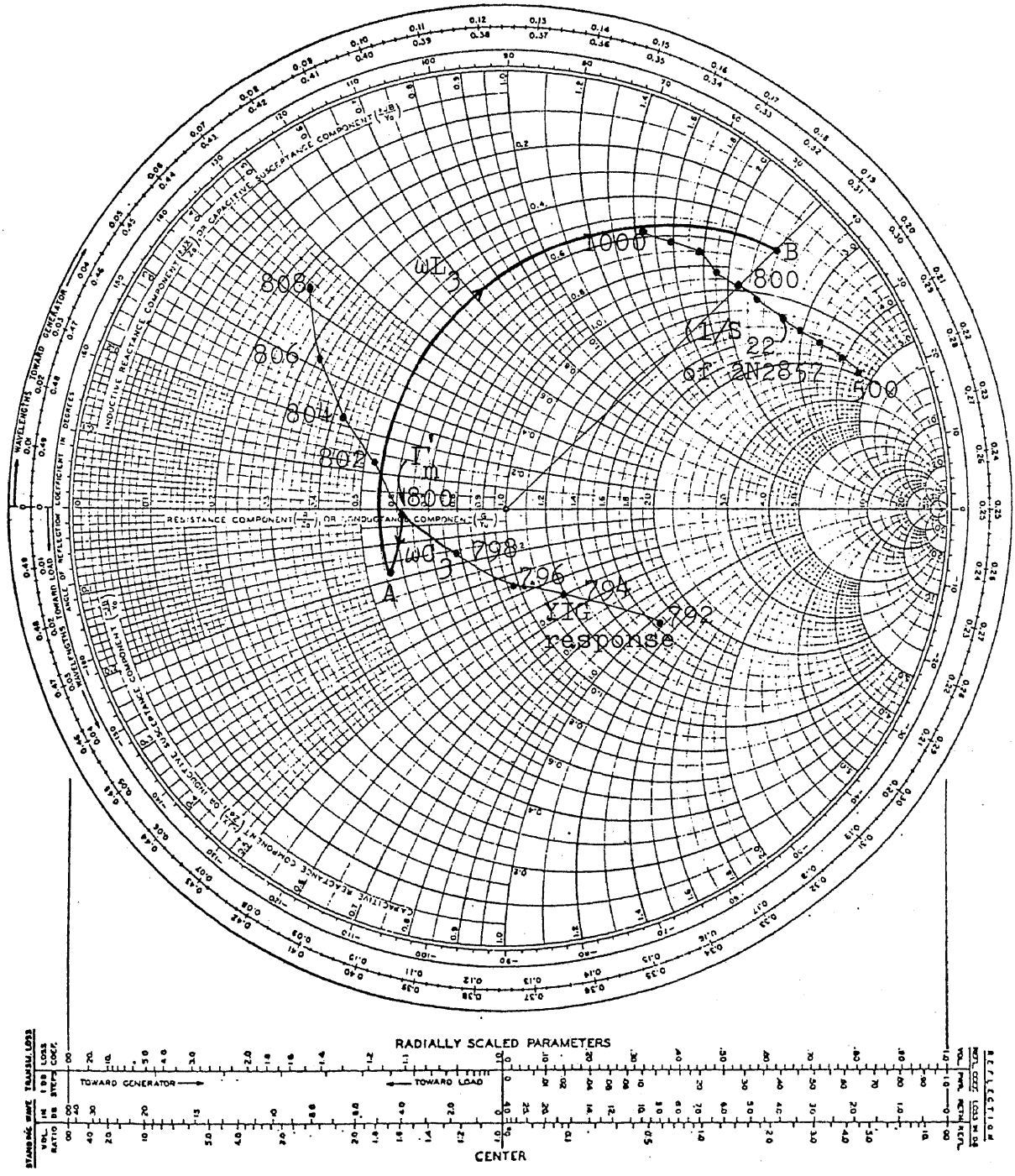

Fig. 4.3.2.d. Smith chart diagram showing transformation which satisfies condition for oscillation at 800 MHZ and electromagnet current I of 46 mA.

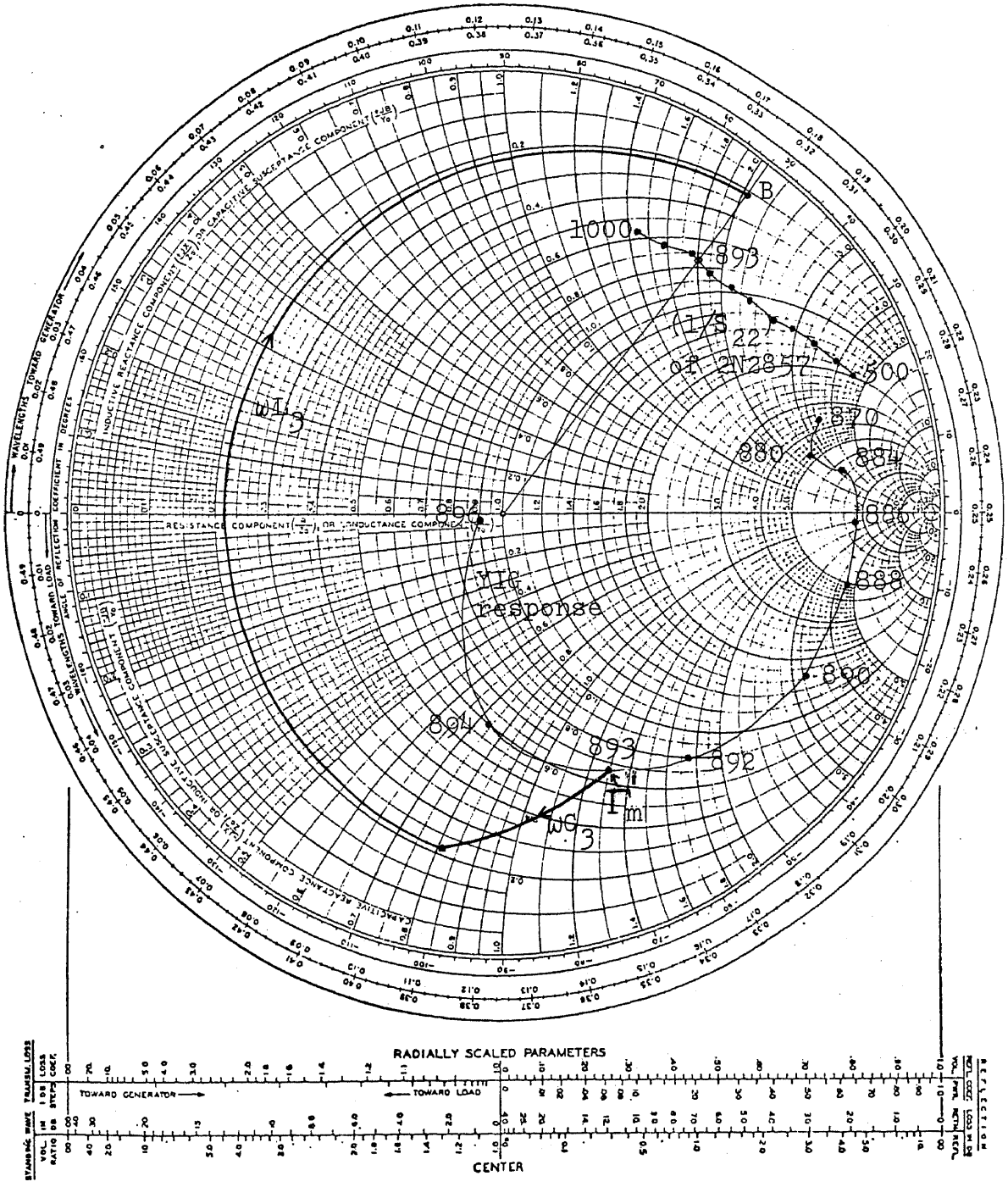

Fig. 4.3.2.e. Smith chart diagram showing transformation which satisfies condition for oscillation at 893 MHZ and electromagnet current I of 52 mA.

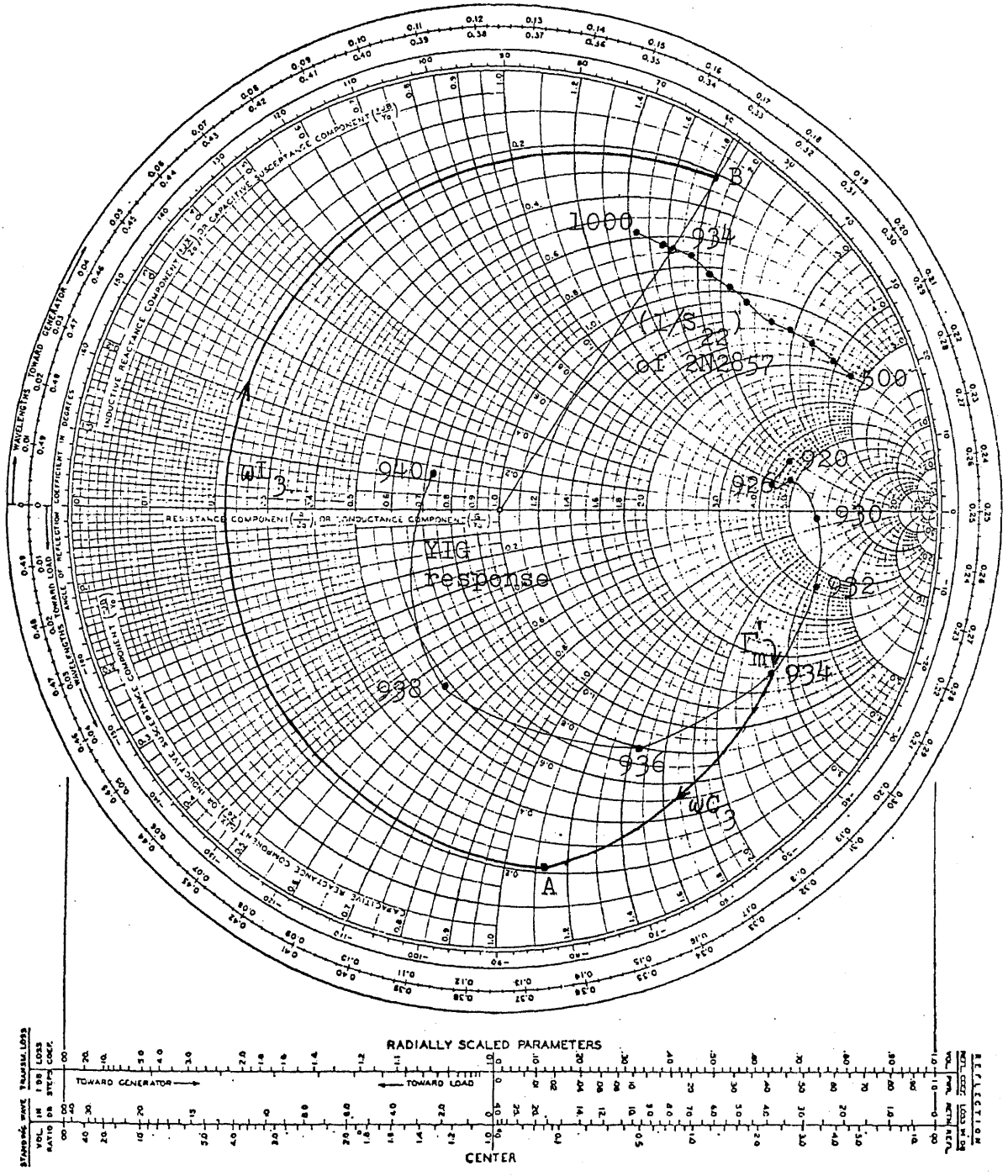

Fig. 4.3.2.f. Smith chart diagram showing transformation which satisfies condition for oscillation at 934 MHZ and electromagnet current I of 55 mA.

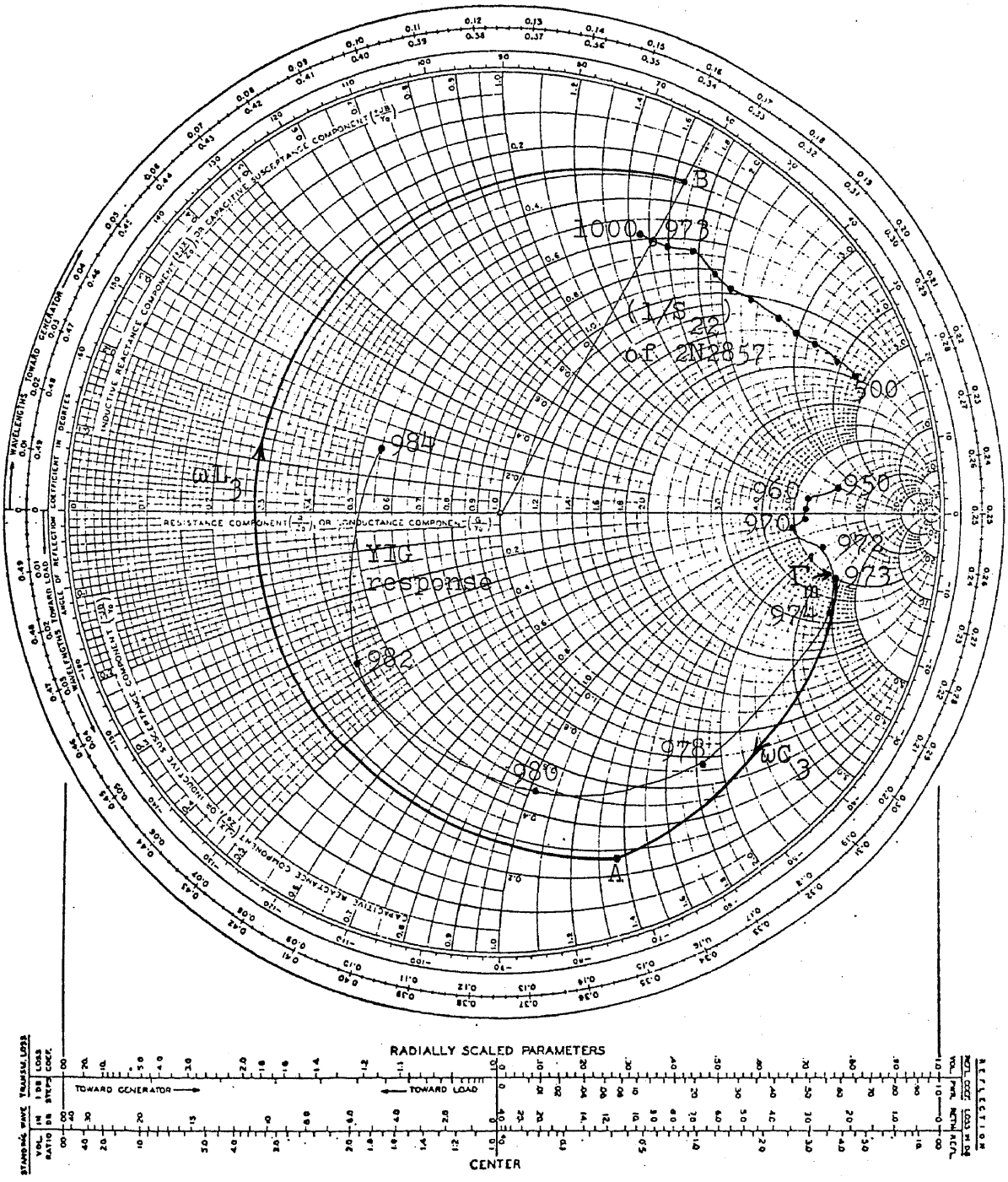

Fig. 4.3.2.g. Smith chart diagram showing transformation which satisfies condition for oscillation at 973 MHZ and electromagnet current I of 58 mA.

circle by the amount ωL_3 until point B is reached [2]. The value of reflection coefficient at this point corresponds to Γ_m in equation (4.2.12.a).

The choice of values for C_3 and L_3 is arbitrary. However, a combination that will satisfy as broad a range of frequencies as possible is desired. Careful consideration and repeated trials give a satisfactory combination such as

$$C_3 = 2 \text{ pF}$$

and

$$L_3 = 25 \text{ nH}.$$

Figure 4.3.3 shows the schematic diagram of the YIG tuned transistor oscillator. Values for the various components are indicated in Table II.

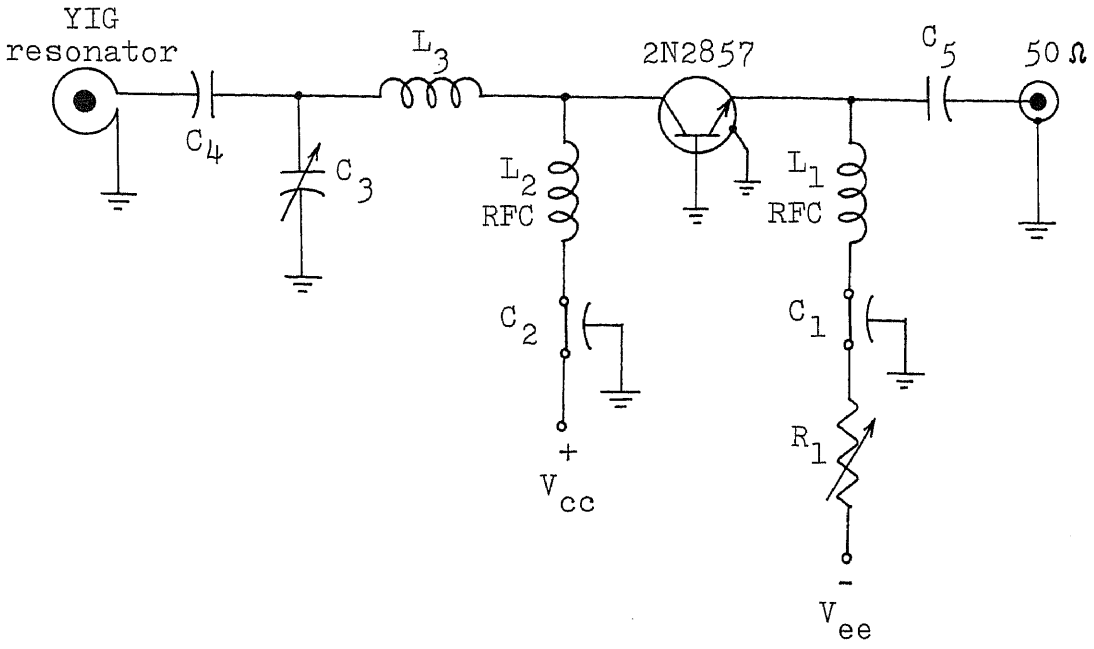

Fig. 4.3.3. Schematic diagram of YIG-tuned transistor oscillator.

TABLE II. Values for Components of Oscillator

R_1 = 1 K pot

C_1, C_2 = 1500 pF Feed-thru

L_1, L_2 = RFC

C_3 = 2 pF

L_3 = 25 nH

C_4, C_5 = 2000 pF

CHAPTER 5

CONCLUSIONS AND RECOMMENDATIONS

A method for designing YIG-tuned transistor oscillators is presented in this thesis. The analysis of the oscillator is based on reflection coefficients measured at network terminals of the transistor and the YIG resonator. The tuning element of the oscillator consists of a YIG sphere enclosed by a loop of wire in a dc magnetic field. The mounting structure that holds the YIG sphere and loop in position is shown in Fig. 5.1.

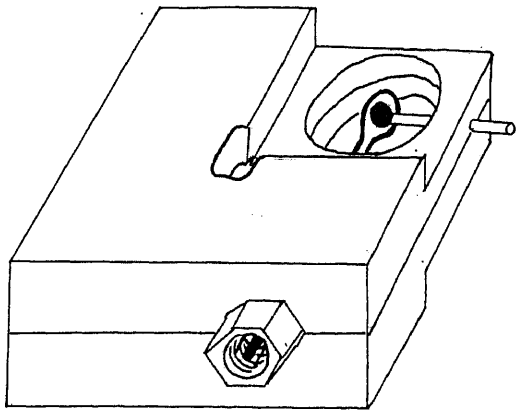

Fig. 5.1. Mounting structure for YIG sphere and coupling loop.

Reflection coefficients measured at the terminals of the YIG tuning element, for various currents through the electromagnet that provides the dc magnetic field, are shown in Fig. 2.4.1. It can be seen that the response of the YIG tuning element to radio frequency signals is similar to that of a parallel LC resonant circuit.

Ideally, a perfect circle with a center at a point on the real axis and the corresponding circumference passing through the zero-impedance point on the Smith chart characterizes a parallel LC resonant circuit. The resonant frequency is the frequency at which the phase of the corresponding reflection coefficient is zero. The normalized resonant resistance at that point can be read directly from the Smith chart.

However, there is a slight rotation in the response curves of the YIG resonator tested, i.e., the center of the open end of the curves does not coincide with the zero-impedance point on the Smith chart. This shift is due to the inductance of the length of transmission line between the loop enclosing the YIG sphere and the connector where the reference plane of all the measurements is located.

In addition, smoother variations of measured reflection coefficients occur in the lower end of the

frequency band. As the frequency of the signal is increased, parasitic modes begin to interfere with the response. These are unwanted resonances which result from non-uniform precessions of the magnetic moments within the YIG sphere. The parasitic modes are represented on Smith charts by small loops along the response curve and a larger loop at the end of the trace. Figures 2.4.1.d through 2.4.1.g show cases where parasitic modes are visible. Therefore, this unit is more suitable for operations in the lower end of the frequency band. One way to reduce such unwanted modes for a given coupling loop size is to use smaller YIG spheres. Such spheres occupy a more concentrated volume where the precession of magnetic moments is more uniform.

The choice of a transistor for the oscillator depends on whether the condition for oscillation can be satisfied. This requirement is met if measured reflection coefficients of the transistor have magnitudes greater than unity over the specified range of frequencies. Otherwise, the transistor must be properly terminated or external feedback must be provided to obtain such a condition. For example, reflection coefficients for signal frequencies from 500 MHZ to 1000 MHZ, measured at the collector terminal of a 2N2857 transistor operating in a common-base configura-

tion, have magnitudes greater than unity when the emitter is connected to a 50-ohm termination. The necessary condition for oscillation is satisfied when the transistor is operated at a quiescent point of V_{ce} = 6 volts and I_c = 12 mA. Thus, the collector terminal of the transistor is connected through an impedance transforming network to the YIG tuning mechanism which is used to control the frequency of oscillation.

In spite of the nonlinear behavior of the YIG tuning unit in the high end of the frequency band, a YIG-tuned transistor oscillator was designed. The circuit is shown in Fig. 4.3.3, and values for the elements in the circuit are listed in Table II. C_1 and C_2 are feed-thru capacitors; L_1 and L_2, RF chokes; C_4 and C_5, dc blocking capacitors. A two element impedance transforming network, consisting of shunt C_3 and series L_3, was chosen to simplify the design and to show how a broadband YIG-tuned transistor oscillator can be designed. This network is used to transform the reflection coefficient or impedance at the output of the YIG tuning element to the required impedance at the collector terminal of the transistor so that the condition for oscillation, specified by equation (4.2.12.a), can be satisfied. Using this network in

the analysis, the relationship between current used to provide the biasing dc magnetic field for the YIG sphere and the frequency of oscillation can be obtained, as shown in Fig. 5.2.

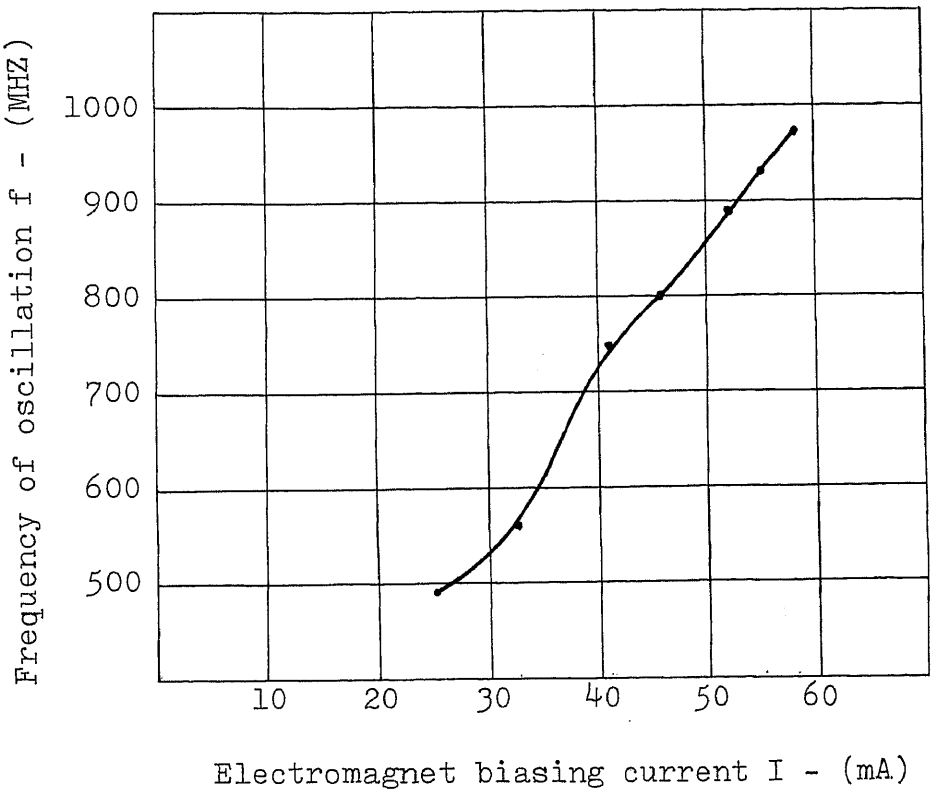

Fig. 5.2. Frequency of oscillation vs. electromagnet biasing current.

In general, the degree of tuning linearity depends upon the complexity of the impedance transforming network and the uniformity in behavior of the YIG tuning mechanism.

Recommendations for Improving Oscillator Circuit

The response of a YIG resonator is highly sensitive to the axial orientation of the YIG sphere with respect to the applied dc magnetic field and the coupling loop. Thus, in order to improve the performance of the YIG tuning mechanism, the possibility of relative motion between the coupling loop and the YIG sphere must be minimized. A possible method of mounting the YIG sphere and connecting it to the external circuitry which should overcome many of the problems of mechanical instability encountered is given below. The coupling loop can be connected directly to the printed-circuit board which is attached to the mounting structure, as shown in Fig. 5.3.

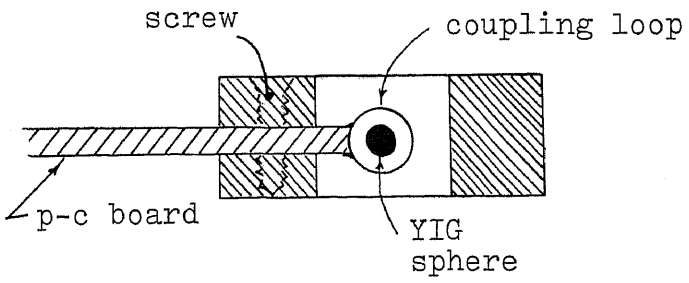

Fig. 5.3. Connection of coupling loop to printed-circuit board.

This will eliminate any twisting of the loop which may occur while tightening connectors whenever they are used. Thus, only attachements for the YIG sphere remain adjustable.

As great difficulties were encountered in orienting the YIG sphere along the desired axis, it is suggested that the rod, with the YIG sphere attached to it, be provided with a graduated knob so that relative locations of axes can be determined from a known axis, for example, an "easy" axis. In addition, a finely threaded rod can be used to hold the sphere so that, once rotated to the desired position, it will stay fixed. Horizontal motion can be compensated by mounting the rod in a sliding block, as shown in Fig. 5.4, so that the rod will not be disturbed while the set screw is being tightened.

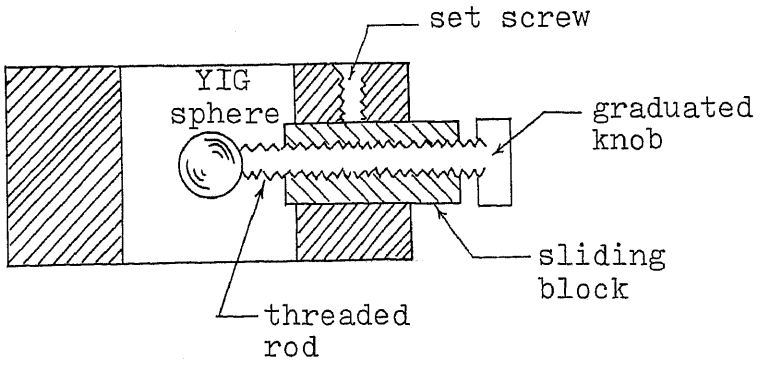

Fig. 5.4. Cross-section of mounting structure with modified features.

Transistor parameters can easily be measured with network analyzers. The fixtures provided for such measurements enable the reference plane to be placed at the base plane of the transistor. However, in actual application, good electrical connections can not be made at the base plane of the transistor without damaging it. Furthermore, biasing networks must be provided to establish the required quiescent point in the actual circuit. Thus, unless the biasing network used is an exact replica of that found in the fixture, the overall parameters will be different. Therefore, it is advisable to use the network analyzer to determine the quiescent point of the transistor such that the condition for oscillation can be obtained, i.e., the presence of a negative resistance region. Then a biasing network is to be designed. Finally, the parameters measured at the terminals of the actual network is to be used for designing the impedance transforming network. This procedure will not only save time but will also give more accurate working data.

Impedance transforming networks can be designed with the aid of Smith charts. Since trial and error method is still used, there may be several possible networks. However, values of components must be

carefully chosen if broadband operation is to be achieved using readily available components. This network links the YIG resonator and the transistor. Because these are basically minute in size, strip line techniques would be most appropriate for implementation, particularly for high frequency broadband operations.

REFERENCES

1. Anderson, E.E., "Some Electrical and Magnetic Properties of Garnets," Journal of Applied Physics, Suppl. to vol. 30, No.4, April 1959, pp. 299s-300s.

2. Anderson, R.W., "S-Parameter Techniques for Faster, More Accurate Network Design," Hewlett-Packard Journal, vol. 18, No. 6, February 1967.

3. Angelo, E.J., Electronics: BJT's, FET's, and Microcircuits. New York: McGraw-Hill Book Co., Inc., 1969, pp. 258-266.

4. Auer, M., "Novel Method to Orient Ferrimagnetic Single Crystal Spheres," IRE Trans., PGMTT-10, January 1962, p.88.

5. Bertaut, F., and F. Forrat, "Structure of Ferrimagnetic Ferrites of Rare Earths," Compt. Rend., vol. 242, 1956, p.382.

6. Carter, P.S., "Side-Wall-Coupled, Strip-Transmission-Line Magnetically Tunable Filters Employing Ferrimagnetic YIG Resonators," IEEE Transactions on MTT, May 1965, pp. 306-315.

7. Carter, P.S., Jr., "Magnetically-Tunable Microwave Filters Using Single-Crystal Yttrium-Iron-Garnet Resonators," IRE Trans. on MTT, vol. MTT-9, May 1961, pp. 252-260.

8. Clark, R.J., and D.B. Swartz, "Take a Fresh Look at YIG-Tuned Sources," Microwaves, February 1972, pp. 40-44.

9. Clark, R.J., and D.B. Swartz, "Combine YIG's with Bulk-Effect Diodes," Microwaves, March 1972, pp.46-53.

10. Comstock, R.L., "Synthesis of Filter-Limiters Using Ferrimagnetic Resonators," Trans. on MTT, November 1964, pp. 599-607.

11. DeGrasse, R.W., "Low-Loss Gyromagnetic Coupling Through Single Crystal Garnets," Journal of Applied Physics, Suppl. to vol. 30, No. 4, April 1959, pp. 155s-156s.

12. Fletcher, P.C., and I.H. Solt, Jr., "Coupling of the Magnetostatic Modes," Journal of Applied Physics, vol. 30, April 1959, pp. 181s-182s.

13. Geller, S., and M.A. Gilleo, "Structure and Ferrimagnetism of Yttrium and Rare-Earth-Iron Garnets," Acta Cryst., vol. 10, 1957, p.239.

14. Helszajn, J., Principles of Microwave Ferrite Engineering. London: Wiley-Interscience, 1969, pp. 1-3.

15. International Telephone and Telegraph Corp., Reference Data for Radio Engineers, 5th. Edition. New York: Howard W. Sams & Co., Inc., 1968, pp. 6-9.

16. Lax, B., and K.J. Button, Microwave Ferrites and Ferrimagnetics. New York: McGraw-Hill Book Co., Inc., 1962, pp. 125-128, 145-158.

17. Matthaei, G.L., "Short-Step Chebyshev Impedance Transformers," IEEE Trans. on MTT, vol. MTT-14, No. 8, August 1966, pp. 372-383.

18. Matthaei, G.L., and L. Young, and E.M.T. Jones, Microwave Filters, Impedance-Matching Networks, and Coupling Structures. New York: McGraw-Hill Book Co., Inc., 1964, pp. 1027-1040.

19. Mercereau, J.E., and R.P. Feynman, "Physical Conditions for Ferromagnetic Resonance," Physical Review, vol. 104, No. 1, October 1956, p. 63.

20. MIT EE Staff, Magnetic Circuits and Transformers. Cambridge, Massachussetts: MIT Press, 1943, pp. 57-81.

21. Sato, Y., and P.S. Carter, "A Device for Rapidly Aligning and Mounting Ferromagnetic Single-Crystals Along Any Desired Axis," IRE Trans on MTT (Correspondence), vol. MTT-10, November 1962, pp. 611-612.

22. Terman, F.E., Radio Engineers' Handbook. New York: McGraw-Hill Book Co., Inc., 1943, pp 48-50.

23. Tokheim, R.E., "Equivalent Circuits Aid YIG Filter Design," Microwaves, April 1971, pp. 54-59.

24. Venator, W., "Charting a Simpler Course to the Design of YIG Filters," Electronics, March 1969, pp. 118-126.